# Invisible threats from typical endocrine disrupting compounds in estuarine environments caused by continuing seawater incursion: *in-situ* evidence of bio-geochemical processes captured by diffusive gradients in thin films

Linzhu Du[a], Wei Guo[a, *], Dongyue Li [a], Martin R. Tillotson [b], Yuhan Zhu [a], Junhui Yue [a], Jun Li[a], Shouliang Huo [c, **], Yue Gao [d], Xu Zhao[e]

[a] National Engineering Laboratory for Advanced Municipal Wastewater Treatment and Reuse Technology, Beijing University of Technology, Beijing, 100124, China

[b] School of Civil Engineering, University of Leeds, Leeds LS2 9JT, United Kingdom

[c] School of Environment, Beijing Normal University, Beijing, 100875, China

[d] Analytical, Environmental and Geo-Chemistry (AMGC), Vrije Universiteit Brussel (VUB), Pleinlaan 2, 1050, Belgium

[e] Institute of Blue and Green Development, Shandong University, Weihai, 264209, China

*Corresponding author: Wei Guo

E-mail address: gwfybj@bjut.edu.cn

Full postal address: Beijing University of Technology, Beijing 100124, China.

**Corresponding author: Shouliang Huo

E-mail address: huoshouliang@126.com

Full postal address: Beijing Normal University, Beijing, 100875, China.

**Abstract:** Continued seawater incursion significantly affects the fate of pollutants in coastal estuaries, yet understanding of the *in-situ* behavior of endocrine-disrupting compounds (EDCs) in these areas remains limited. The distribution, transport and microbial response of two model EDCs, bisphenol A (BPA) and nonylphenol (NP), in three estuarine zones of slight (SZ), moderate (MZ) and complete (CZ) seawater incursion were investigated *in-situ*. Results showed seawater incursion reshaped the environmental gradients of the coastal estuaries on a spatial scale. Varying salinity gradient and tidal hydrodynamic conditions altered the dependence of EDCs on organic carbon, and promoted the release of accumulated EDCs from estuarine sediments resulting in the lowest residues of BPA (2.74 ± 0.76 μg/kg) and NP (10.25 ± 5.86 μg/kg) in the MZ. The resupply potential of BPA ($R$ = 0.171 ± 0.058) and NP ($R$ = 0.107 ± 0.015) from sediment to porewater was significantly higher in the SZ than in other zones ($p$<0.001), due to both higher contaminant accumulation in this zone and inhibited resupply in MZ and CZ caused by seawater incursion. Furthermore, seawater incursion significantly reduced the microbial community diversity in the CZ ($p$<0.001), being dominated by *Vibrio* (67.00 ± 1.13%), and accordingly weakened the ability to transform organic matter in this region. Based on predicted sea level rise and the transport characteristics of EDCs under increased seawater incursion, it is estimated that the cumulative additional release of BPA and NP in the estuary will reach 1.8 and 1.5 tons by 2100, respectively. In order to mitigate the risk of additional estuarine EDCs release due to seawater incursion, increasing vegetation cover, strict monitoring, and

climate policy interventions may be effective strategies.

**Keywords:** Seawater incursion, estuarine sediment, endocrine disrupting compounds, *In-situ*, microbial communities.

## 1. Introduction

Endocrine-disrupting compounds (EDCs) are examples of refractory organic micropollutants distributed widely in the environment and exhibiting a variety of complex and concerning characteristics (Yan et al., 2022). For example, EDCs can cause irreversible effects on the reproductive and development systems of animal life (Yuan et al., 2017a), and annual productivity loss due to EDC exposure is estimated to cost over US$40 billion (Zeng et al., 2024). Bisphenol A (BPA) and nonylphenol (NP) are typical EDCs extensively used as raw materials in the production of consumer products such as surfactants, plastics and food containers (Xiao et al., 2023); both have been listed as priority pollutants by the European Union (EU) (Wang et al., 2016). The annual consumption of NP ranges between 25 and 50 kilotons in the EU (Chen et al., 2019), and global production for BPA increases from 2.8 million $t \cdot year^{-1}$ in 2002 to more than 8 million $t \cdot year^{-1}$ in 2024 (Paolella et al., 2024). As a result, large amounts of BPA and NP (BPA, in particular, more than 2,000 $t \cdot year^{-1}$) entered the aquatic environment through wastewater discharge and rainfall runoff to waterbodies (Lee et al., 2020). Through these vectors, BPA and NP may spread over huge distances in the aqueous environment in either dissolved or solid forms due to their hydrophobic, persistent, and bio-accumulative characteristics (Du et al., 2025). Subsequently, these

43 compounds pose a serious threat to aquatic organisms. Long-term exposure to
44 environmentally relevant concentrations of NP (1.0 μg/L) and BPA (0.1 μg/L) has been
45 shown to impair the immune system of fish (Lee et al., 2013; Qiu et al., 2016). Moreover,
46 some studies have confirmed that simultaneous exposure to BPA and NP may lead to
47 additive or synergistic toxicity (Wu et al., 2011; Huang et al., 2017, 2018). Additionally,
48 BPA and NP can significantly alter the microbial community structure in depositional
49 environments and reduce microbial diversity (Yuan et al., 2017b; Zoppini et al., 2020).
50 Under aerobic environments, they can readily involve in microbial metabolic processes,
51 potentially influencing the succession of microbial communities in sediments (De
52 Weert et al., 2010; Bradley et al., 2016; Zoppini et al., 2018). Currently, BPA and NP
53 are considered to be the main EDC pollutants in the marine environment, and present a
54 continued challenge to the viability of marine species such as dolphins, cetaceans and
55 pelagic fish, etc.(Luo et al., 2024).

56 Coastal estuaries are key channels for material cycling between terrestrial and marine
57 environments, and are amongst the most fragile and economically important
58 ecosystems on the planet (Kirwan and Megonigal, 2013). Estuaries are also important
59 reservoirs in the retention, storage, and release of pollutants into the marine
60 environment (Yuan et al., 2017a). Once released into estuaries, BPA and NP tend to
61 partition preferentially into organic matter in the sediment (Lee et al., 2013). This is
62 particularly evident for NP, which is subject to significant accumulation in sediments
63 due to its high hydrophobicity (Log $K_{ow}$ = 5.76) and strong soil/sediment sorption

capacity (Log $K_{oc}$ = 4.48–5.6) (Lee et al., 2013). Although BPA is only moderately hydrophobic (Log $K_{ow}$ = 3.32), it still accumulates extensively in sediments. This may be attributed to the presence of two benzene rings in BPA, which promote strong π–π interactions with organic matter and increase its affinity for sedimentary organic carbon pore sites (Sun et al., 2010). As a result, BPA also exhibits a high soil/sediment adsorption coefficient (Log $K_{oc}$= 2.5–3.18). In addition, the salting-out effects further enhance the sorption of BPA and NP on marine sediments, resulting in their accumulation rates in marine sediments that are least 1,000 times higher than in other environmental compartments (Safakhah et al., 2020). Thus, with the continuous anthropogenic use and discharge of BPA and NP (Chen et al., 2019; Lee et al., 2020; Xiao et al., 2023), estuaries as recipients of terrestrial pollution will accumulate significant amounts of these contaminants(Chen et al., 2019), ultimately becoming important sinks and sources of BPA and NP in their own right (Omar et al., 2017). Indeed, several studies have revealed that BPA and NP contamination levels in estuarine sediments is extremely high. For example, surface sediments of Thane Creek in India contained 35.8 μg/kg and 537.8 μg/kg BPA and NP, respectively (Tiwari et al., 2016), and, in the Pearl River Estuary in China, concentrations of BPA and NP in sediments reached 13.2 μg/kg and 20.8 μg/kg, respectively (Diao et al., 2017).

Additionally, as sea levels rise due to global warming, the problem of seawater extension into estuaries is becoming an increasingly important global concern (Tang et al., 2020). By 2100, coastal estuaries could lose up to 30% of their area, threatening

85 approximately US$27 trillion of ecological economic activity (Schuerch et al., 2018;
86 Saintilan et al., 2022). At the same time, seawater incursion will also alter
87 biogeochemical processes in estuarine sediments. When seawater incursion occurs,
88 sediments are frequently washed away, and strong tidal hydrodynamics result in
89 continuous re-release of legacy pollutants accumulated in estuarine sediments,
90 enhancing their mobility and bioavailability (Fetters et al., 2016). Furthermore, with
91 tidal pumping and advective transport of oxygenated seawater, the oxygenation
92 capacity of sediment is enhanced (Huettel et al., 2018) which enhances aerobic
93 microorganism activity in the sediment (Anschutz et al., 2009). Once seawater
94 incursion is completed, sediments may be permanently submerged by seawater, and the
95 evolution of microbial communities in the sedimentary aquifer will be achieved. Thus,
96 nitrogen reduction process (such as denitrification and anammox) will also increase
97 (Xiong et al., 2023). In this manner, the intensification of seawater incursion will affect
98 pollutants in estuarine zones to different degrees, hence they will exhibit different
99 environmental and geochemical behaviors. This can lead to a number of unforeseen
100 environmental risks and consequences. Although previous studies have focused on the
101 fate of some inorganic pollutants such as nitrogen, phosphorus and heavy metals in
102 estuaries under the influence of seawater incursion (Chakraborty et al., 2019; Zhang et
103 al., 2023a). There is a lack of research on the migration and transformation behavior of
104 refractory organic pollutants such as EDCs in estuarine areas under the influence of
105 seawater incursion, especially at the sediment-water interface (SWI) in areas affected

106 by different degrees of seawater incursion. In addition, to the best of our knowledge,
107 most studies still focus on investigating the concentration distribution of pollutants and
108 assessing ecological risk by comparison them with some environmental quality
109 standards (Chiriac et al., 2021; Zainuddin et al., 2023). However, fewer researches have
110 been conducted on the prediction of pollutant releases fluxes at SWI under dynamically
111 changing environmental conditions, even though this is directly related to the
112 bioavailability of pollutants. The exploration of these problems is considered important
113 for the ecological and environmental security of the estuary. Therefore, further analysis
114 of the distribution, diffusion and transformation of EDCs in the estuarine environment
115 under seawater incursion is of significant scientific value for understanding the
116 comprehensive effects of seawater incursion and EDC input on estuarine ecosystems.
117 Sediments, unlike water bodies, are heterogeneous and more likely to host various
118 biogeochemical processes at the microscale (Lin and Pan, 2023). Thus, small changes
119 in the sedimentary environment can lead to significant changes in the form and
120 concentration of pollutants in sediments, especially at the SWI (Liu et al., 2022a). A
121 precise study of pollutant exchange mechanisms at the SWI will be helpful in
122 understanding the source-sink relationship between sediments and estuarine waters
123 under the influence of seawater incursion, and assessing the bioavailability of pollutants
124 (Chen et al., 2022). However, recent studies on the pollution process and the release
125 flux of pollutants at the SWI usually use active sampling methods (i.e., "*ex-situ*"
126 methods) (Puttonen et al., 2024). These methods disturb the *in-situ* sediment

127 environment, disrupt the equilibrium of contaminant distribution in the sedimentary
128 environment, and fail to capture the dynamic information on pollution under changing
129 environmental conditions (Li et al., 2023a). These disadvantages can cause
130 considerable analytical error, and result in major deviations between experimental
131 observations and the real world situation, which in turn affects our understanding of
132 pollution behavior and risk assessment (Gao et al., 2016). The Diffusive Gradients in
133 Thin film technique (DGT) is an innovative passive sampling method, and can be used
134 to determine the diffusion and exchange of pollutants at the SWI based on Fick's first
135 Law (Arsic et al., 2018). More importantly, DGT can capture the labile fractions of
136 pollutants (including the free fraction and the fraction that can be released from the
137 environment medium), thus providing a more accurate representation of the
138 bioavailability of pollutants than total concentration measurements (Liang et al., 2023).
139 To date, DGT has been used to obtain information on the *in-situ* release of organic
140 micropollutants such as pesticides and antibiotics in sediments (Chen et al., 2014; Li et
141 al., 2021). Therefore, the DGT technique could help us obtain *in-situ* dynamic exchange
142 processes and bioavailability characteristics of EDCs at the estuarine sediment-water
143 interface (ESWI), especially under changing environmental conditions, e.g., as affected
144 by seawater incursion.

145 In this study, active sampling and DGT were used in combination to investigate the
146 *in-situ* fate of typical EDCs such as BPA and NP in the ESWI under the influence of
147 seawater incursion. Sediment cores from slight (SZ), moderate (MZ) and complete (CZ)

estuarine zones of seawater incursion were collected. The interfacial distribution and diffusion of both BPA and NP, as well as the potential correlations between microbial communities and these two EDCs at the three different estuarine zones were analyzed. In addition, a release model of estuarine EDCs due to seawater incursion caused by sea level rise was also established. Thus, the main objectives of our study were as follows: 1) to clarify the impact of seawater incursion on the *in-situ* distribution of BPA and NP in estuarine sediments; 2) to investigate the impact of seawater incursion on the diffusion characteristics of BPA and NP in sediments; 3) to elucidate the influence of seawater incursion on microbial community succession in sediments and microbial responses to the fate of BPA and NP; and 4) to further assess the possible risk of EDC release from estuarine sediments due to sea level rise.

## 2. Materials and Methods

### 2.1 Sampling area, DGT field deployment, and sample collection

Frequent seawater incursion into estuaries due to global sea level rise has resulted in threats and losses to groundwater, agriculture, drinking water safety, and coastal bird habitats (Mondal et al., 2023; Lee et al., 2024; Su et al., 2024; van de Pol et al., 2024). The latest research also confirms that seawater incursion is a prominent problem in China's coastal estuarine areas (Wang et al., 2022). Amongst these, the Liaohe estuary in northern China, a semi-enclosed estuary suffering from relatively poor diffusion conditions, has experienced serious coastal vegetation degradation and soil salinization problems due to seawater incursion (Ma et al., 2019; Guo et al., 2022). Thus, the Liaohe

estuary was chosen to study the fate of organic pollutants in estuarine areas caused by seawater incursion. The sample collection and DGT deployment were carried out at Red Beach on the Liaohe estuary (Fig. S1 and S2; 120°44′6.67″E, 40°33′41.66″N). The discharge of runoff from the Liaoehe estuary into the sea has long been regulated by the upstream sluice tidal gate, the average runoff is 1.2-1.3 billion·$m^3$ monthly (Hu et al., 2023; Dong et al., 2024). Red Beach is located in the wetland reserve of Huludao City in China, with area 600 hectares, most of the area is bare, flat and tidal. Tidal action, which is common in coastal areas, plays a crucial role in facilitating the diffusion and transport of sediment particles, nutrients, and pollutants across the tidal flats (Gu et al., 2024). According to the (Liaoning Provincial Marine Ecological Early Warning Monitoring Bulletin (2023), 2024), the tide at Red Beach is in a semidiurnal state with a tidal range of 2–3 m. The average annual temperature in the region is 10°C and the average annual precipitation and evaporation are 600 mm and 1500 mm, respectively. Estuarine pollution mainly comes from terrestrial runoff from industrial and agricultural activities in the upper reaches of tributary rivers (Guo et al., 2022). Since Red Beach is located in a nature reserve there are no significant urban or industrial developments nearby, which avoids potential human disturbance. Hence, the sedimentary environment in Red Beach may be deemed as relatively stable and well preserved.

Based on the environmental conditions and seasonal characteristics of Red Beach, the sampling activities was selected to be conducted during the flat-water period from

late July to the end of August 2024. During this period, the upstream sluice was closed, causing the river flow to be generally less than 0.3 billion·$m^3$ monthly, resulting in very low runoff. And seawater incursion typically occurred during low runoff periods, extending approximately 5-10 km upstream of the estuary (Hu et al., 2023; Dong et al., 2024). Furthermore, this period is characterized by moderate evaporation (average 600 mm) and relatively active microbiological activity (average temperature 19.5°C) (Huludao Environmental Quality Report, 2024), which facilitates sample collection, DGT placement and the conduct of studies on seawater incursion (Li et al., 2023b; Hlaing et al., 2024; Gao et al., 2025). In order to more objectively assess the impact of seawater incursion on the release of EDCs, three sampling campaigns were conducted, with each sampling event lasting one week. During each sampling period, samples were collected from three zones (SZ, MZ, and CZ) along the direction of seawater incursion to reveal the impact of the degree of seawater incursion. DGT was deployed simultaneously to represent the characteristics of slight, moderate and complete incursion (Fig. S1). According to field survey, under tidal influence, SZ and MZ were inundated by seawater for between 3 and 5 h, and 12 and 15 h per day, respectively, while CZ was permanently inundated by seawater. The distance between each sampling zone was about 500 m. Three sites were selected within each sampling zone to eliminate spatial heterogeneity, and the distance between these sites was about 30 m. Subsequently, one DGT sediment probe (DGT-HLB) for BPA and NP, and one DGT sediment probe (DGT-Chelex100/AgI) for iron (Fe), manganese (Mn), and dissolved

211 sulfur (S) were deployed *in-situ* at each site at ebb tide. Each type of DGT was deployed
212 in three parallel replicates (Fig. S2). The details of the above DGT composition are
213 described in Text S2. When deploying DGT probes, the tidal flats of SZ and MZ were
214 exposed, and the water depths of the CZ was between 0.5 and 1.0 m. In the SZ and MZ,
215 the entire window area of the DGT probes was slowly inserted vertically and directly
216 into the sediment bed by 15 cm. In the CZ, the DGT probes were attached in the bottom
217 of perforated plexiglass profiles (thickness: 3 cm, width: 3 cm, length: 120 cm). Then,
218 in each site, six separate profiles with attached probes were slowly inserted into the
219 sediment bed by 15 cm, and protected by six stone supports in each site (Fig. S3). All
220 probes in the three zones were fully inserted for one week, experiencing a total of about
221 14 tidal cycles. At the last ebb tide the DGT probes were recovered, and were then
222 washed with Milli-Q (MQ) water and placed into sealed bags. At the beginning and end
223 of each sampling period, four sediment cores (~25 cm) adjacent to the DGT probes in
224 each zone were collected from the three sites using a 10-cm diameter PVC sampling
225 tube. No bioturbation was observed in all collected sediment cores, and the SWI of the
226 obtained sediment cores was clear. An additional sediment sample was also collected
227 at each station using a small shovel to determine the effect of matrix on extraction and
228 concentration recoveries. Finally, the sediment cores, recovered DGT probes, and
229 surface sediments were immediately stored in sample boxes with ice packs prior to
230 transportation to the laboratory.

231 **2.2 Sample treatment and analysis of physicochemical properties**

In the laboratory, the sediment cores were carefully divided into 1-cm portions and centrifuged at 3,000 rpm for 40 min to obtain porewater. After centrifugation, the residual sediments were freeze-dried, ground, and sieved (100-mesh) for subsequent analysis. BPA and NP analyses were performed on three sediment cores collected at the beginning and end of each sampling event, and the mean average was used as result. The remaining sediment core was used for sediment environmental factor analysis. Total organic carbon (TOC) in sediment was measured using the combustion oxidation-titration method (Du et al., 2025). The salinity and pH values of each sediment slice were determined using a water quality tester (WTW GmbH, Germany). Before measurement, dry sediments were mixed with MQ water at a ratio of 1:5 for salinity and 1:2.5 for pH (Yu et al., 2022).

## 2.3 Extraction of BPA and NP from Samples

### 2.3.1 DGT

The details of DGT samples' extraction were described in our previous study (Du et al., 2024, 2025). Briefly, in the laboratory, the DGT gel was cut along the window area using a Teflon blade. For DGT-HLB, the binding gel was divided into 1 cm segments, and each segment was transferred to 10 mL glass centrifuge tube. Then, 8 mL of acetone was added to the tube, sonicated for 40 min, and centrifuged at 3500 rpm for 10 min to extract the target substances from the binding gel. The same procedure was repeated twice for the residual gel, then the extracts were combined and evaporated to dryness under a gentle flow of nitrogen gas. Subsequently, 1 mL of methanol was added to the

dry residue to redissolve the target compound. The internal standard (BPA-d16 and NP-d4) was introduced into the tube, vortexed, and then filtered using a 0.22-μm PTFE filter (Aladdin, Shanghai, China) into 2 mL LC vials, which were stored at -20°C until LC-MS analysis. For DGT-Chelex100/AgI, the AgI diffusion gel and Chelex100 binding gel were together peeled from the probe. Next, the AgI gel was scanned using a flat-bed scanner (HP 3100) for analysis of dissolved S. The Chelex100 gel was sliced into 5 mm segments, and each segment was placed in a glass centrifuge tube containing 0.4 mL of 1 M $HNO_3$ for 24 hours to elute, then stored carefully prior to ICP-MS analysis.

**2.3.2 Porewater**

Porewater extraction methods were based on our previous research with some modifications, and procedures are described in Supporting Information (SI), Fig. S4. Briefly, 1 mL of porewater was diluted to 150 mL using MQ water to reduce matrix concentration and minimize error. The diluted solution was filtered through a glass fiber membrane (47 mm, Aladdin, Shanghai, China) and then concentrated by solid-phase extraction (SPE) as described in the SI (Text S3). Each sample was tested in triplicate. The concentration of BPA and NP extracted from porewater is denoted as $C_d$.

**2.3.3 Sediments**

Sediment extraction methods were based on our previous research with some modifications, and procedures are described in the SI, Fig. S4. Briefly, 1.0 g of sediment was transferred to a 10-mL glass tube with 8 mL acetone, sonicated for 40 min, and

centrifuged at 3500 rpm for 10 min to extract BPA and NP. This was repeated a second time, and the extracted supernatants combined and evaporated to 1-2 mL under a gentle stream of high-purity nitrogen, diluted to 150 mL with MQ water (acetone content <1%, V/V), prior to further processing. The diluted extracts were filtered (47 mm glass fiber membrane, Aladdin, Shanghai, China) and purified by SPE (Text S3). Each sample was tested in triplicate. The concentration of BPA and NP of the sediment is denoted $C_s$.

**2.4 Diffusion analysis of BPA and NP in sediment**

The binding layer in the DGT acts as a sink for compounds in the sediment porewater/water, where an induced flux from the sediment/water passes through the diffusive layer and is bound in the binding layer (Ji et al., 2022). Thus, the diffusion characteristics of pollutants at the SWI may be monitored *in situ* by DGT. The ratio $R$, an index reflecting depletion of sediment porewater concentration to the DGT interface, was introduced to characterize the magnitude of this diffusion and resupply. Typically, higher values of $R$ indicate a stronger capacity of resupply from sediment to porewater (Du et al., 2025). And three scenarios of the resupply capability were determined based on the $R$ values. (i) $R > 0.95$, the target substances are fully resupplied from sediment to porewater; (ii) $0.1 < R < 0.95$, the target substances are partially resupplied from sediment to porewater; (iii) $R < 0.1$, there is diffusion only, with very limited resupply from the sediment to porewater. Moreover, the values of $R$ in sediments can be impacted by various environmental factors, such as the labile pool size of target substances and particle concentration ($P_c$, the ratio of the mass of total sediment solid particles to the

volume of total porewater) (Li et al., 2021). In this study, the diffusion process of BPA and NP in sediments was quantified using $R$ as follows(Chen et al., 2014):

$$R = \frac{C_{DGT}}{C_d} \quad (1)$$

where $C_{DGT}$ is the time-weighted average concentration of BPA and NP in DGT (Eq. 2):

$$C_{DGT} = \frac{M\Delta g}{DAt} \quad (2)$$

where $M$ is the mass of BPA and NP bound in the DGT (Text S4), $\Delta g$ is the thickness of the diffusion layer in mm, $D$ is the diffusion coefficient of BPA and NP in $cm^2 \cdot s^{-1}$, $A$ is the exposed area of DGT in $cm^2$, and $t$ is the deployment time, s.

**2.5 Characterization of microbial community in sediment**

To further evaluate the impact of seawater incursion on the microbial communities in sediments at different depths, the sediment cores were classified into four depth intervals, as referred to by a number of previous studies (Zhang et al., 2021; Gong et al., 2022; Wang et al., 2024a): Part 1 (0 ~ -4 cm), Part 2 (-5 ~ -8 cm), Part 3 (-9 ~ -12 cm), and Part 4 (-13 ~ -15 cm). Three replicate sediment samples (1.0 g, wet weight) were collected from each part and preserved at −80 °C prior to high-throughput sequencing. Genomic DNA was extracted from the sediment using OMEGA Soil DNA Kit (M5635-02) (Omega Bio-Tek, Norcross, GA, USA). PCR amplification of the bacterial 16S rRNA gene V3–V4 region was performed using the forward primer 338F (5'-ACTCCTACGGGAGGCAGCA-3'). Libraries were constructed using the Illumina TruSeq Nano DNA LT Library Prep Kit. The constructed libraries were quantified using a Quant-iT PicoGreen dsDNA Assay Kit, and high-throughput sequencing was

316 performed on an Illumina NovaSeq-6000. Taxonomic assignment of amplicon
317 sequence variants (ASVs) was conducted using a Silva 138.1 database. The raw 16S
318 rRNA gene reads were deposited on the NCBI Sequence Read Archive database with
319 the accession number PRJNA1201922.

320 **2.6 Construction of predictive models for BPA and NP release with sea level rise**

321 A simple release prediction model of BPA and NP from sediment to seawater during
322 the 2024-2100 period under different sea level rise scenarios was developed, by
323 referring to previous methods with minor modifications (Stigebrandt et al., 2014; Lu et
324 al., 2021; He et al., 2023). The derivation and details of model construction are
325 described in SI (Text S5). The model was constructed to predict cumulative additional
326 releases of BPA and NP from the perspective of the ESWI considering both the loss of
327 coastal wetland area and the net release fluxes of BPA and NP. Briefly, (i) the DGT-
328 labile concentration gradients of BPA and NP in the vicinity of the SWI was used to
329 estimate the apparent diffusion flux of BPA and NP across the SWI. It was calculated
330 as the sum of the diffusion flux of BPA and NP from the overlying water to the SWI,
331 and from the sediments to the SWI; (ii) the function of additional estuarine area loss
332 and seawater incursion time was determined by referring to previous studies (Mengel
333 et al., 2016); (iii) the cumulative additional release over time was determined by
334 multiplying the integral of the function of estuarine area and seawater incursion time
335 with the release flux. Based on the above steps, Equation 3 was established to estimate
336 the cumulative increase in BPA and NP over time starting from 2024 to the

corresponding year of different sea level rise scenarios under continuous seawater incursion:

$$P = [-D_w(\frac{\delta C_{DGT}}{\delta x_w})_{(x=0)} - \varphi D_s(\frac{\delta C_{DGT}}{\delta x_s})_{(x=0)}] \cdot \int_{2024}^{T} f(T) \quad (3)$$

where $P$ is the projected increase in release of BPA and NP over time in tones, $D_w$ and $D_s$ are the diffusion coefficients of BPA and NP ($cm^2 \cdot s^{-1}$), respectively, in the overlying water and sediment, $(\frac{\delta C_{DGT}}{\delta x_w})_{(x=0)}$ and $(\frac{\delta C_{DGT}}{\delta x_s})_{(x=0)}$ are the DGT-labile concentration gradients in the overlying water and sediment in $ng \cdot mL^{-1} \cdot mm^{-1}$, respectively. A distance of 1 cm from the SWI to the sediment was used to fit the gradient, $\varphi$ is the porosity of the sediment, $T$ is time of seawater incursion in years, and $f(T)$ is defined as the loss of coastal estuarine area as a function of time.

**2.7 Data analysis and quality assurance**

BPA and NP were analyzed by LC-MS with details in Text S6. Briefly, they were identified using an Agilent 1290 Infinity/6460 LC/QQQ MS operated in negative multiple reaction monitoring (MRM) mode. LC separation was achieved with a Poroshell 120 EC-C18 (1000 bar, 3 mm×150 mm, 2.7 μm, Agilent). The mobile phase consisted of phase A (Milli-Q water with 0.025% ammonia) and phase B (methanol with 0.025% ammonia) with a flow rate of 0.4 mL/min. The gradient elution program was 20% B kept to 1 min, then increased to 100% B at 3 min and kept constant for 4 min. Followed by returning to the initial conditions within 1 min. Finally, the column was re-equilibrated for 2 min. The column temperature was kept at 40℃, and the injection volume was 20 μL. The MS parameters were given in Table S4.

Fe and Mn in DGT were analyzed by ICP-MS (Optima8300, PerkinElmer). Dissolved S concentration was obtained through Computer-Imaging Densitometry (Text S7). Details of quality assurance/quality control are available in SI (Text S8). Variations in the profile distribution of BPA, NP, and environmental factors were plotted using OriginPro 2024. Data obtained from DGT and the active sampling method were checked for normality and homogeneity using Levene's test. Since the data did not satisfy a normal distribution and did not show homogeneous variances, the non-parametric Kruskal-Wallis test was used to check for significant differences (significance at $p<0.05$) between BPA and NP profiles, and between SZ, MZ and CZ (Chen et al., 2024). Co-occurrence networks were constructed by the top 500 ASVs of SZ, MZ and CZ sediments using Cytoscape and Gephi (Chen et al., 2024).

## 3. Results

### 3.1 Physicochemical parameters of sediments in different zones

Fig.1 shows the variation of physicochemical parameters in the sediment profiles of SZ, MZ and CZ. DGT measurements reflect the labile fractions of elements in the sediment. The results confirm the lowest labile fractions of Mn, Fe and $S^{2-}$ in the MZ (Mn: 96.33 ± 2.21 μg/L; Fe: 129.56 ± 2.57 μg/L; $S^{2-}$: 3.92 ± 3.19 mg/L). Typically, the accumulation of dissolved Fe, dissolved Mn and S in the sediments indicate a successive reduction of Fe(III), Mn(III/IV) and sulfate occurred with increasing oxygen depletion (Pan et al., 2021). The profiles of Fe, Mn and $S^{2-}$ in the sediments indicated anoxic conditions in the SZ and CZ, and relatively aerobic conditions in the MZ. The

pH values in the SZ, MZ and CZ sediment profiles all decreased with increasing depth, ranging from 8.61 to 8.88, 8.57 to 8.84 and 8.32 to 8.46, respectively. TOC and salinity in the SZ, MZ and CZ sediment profiles all increased with increasing depth; TOC in the range of 0.34 - 0.52 %, 0.32 - 0.61 % and 0.37 - 0.56 %, respectively, and salinity in the range of 2.27 - 3.98 ‰, 2.02 - 4.26 ‰ and 2.28 - 5.45 ‰, respectively. In short, the extent of seawater incursion resulted in significantly different environmental factors in the SZ, MZ and CZ sediments (Fig. S5). Greater salinity (4.14 ± 0.77 ‰) and TOC (0.45 ± 0.07 %) accumulated in CZ sediments, whereas the pH of SZ sediments was higher (8.72 ± 0.07).

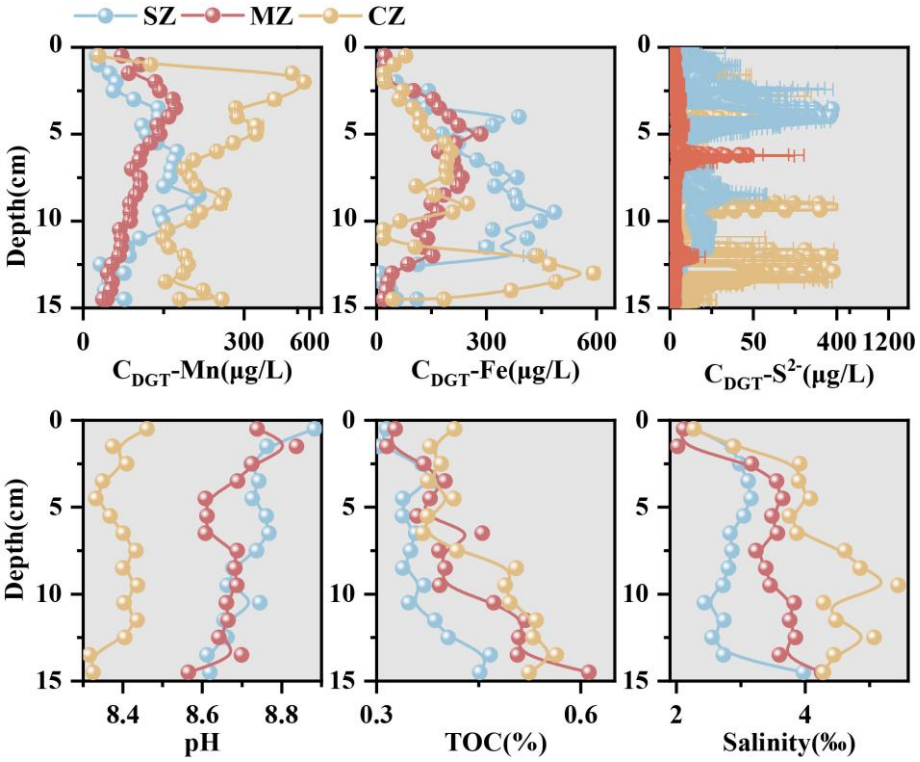


**Fig. 1** Physicochemical parameters in the sediment profiles of SZ, MZ and CZ.

### 3.2 Variations in BPA and NP concentration in sediment from different zones

Fig. 2 shows the profile variations of BPA and NP in the sediment, porewater and

DGT of the SZ, MZ and CZ. In the sediment profile, NP concentrations in the SZ, MZ and CZ decreased with increasing depth, ranging from 44.44 to 11.45 μg/kg, 24.85 to 4.99 μg/kg, and 36.88 to 7.23 μg/kg, respectively. BPA concentrations fluctuated with depth in the SZ, MZ and CZ, with average concentrations of 7.09 ± 2.46 μg/kg, 2.74 ± 0.76 μg/kg, and 3.35 ± 0.81 μg/kg, respectively. Overall, NP concentrations in sediment were higher than BPA concentrations in all three zones, which was attributed to higher hydrophobicity ($\log K_{ow}$=5.76) and dissociation constant ($pK_a$=10.3) of NP, which tended to accumulate on solid particles ($K_d$= 3.07 ~ 19.49 g/mL, Table S2). For the porewater and DGT profiles, BPA and NP concentrations fluctuated with depth in the SZ, MZ and CZ. In these three zones, the average DGT concentration of BPA was 0.45 ± 0.12 μg/L, 0.11 ± 0.03 μg/L, and 0.14 ± 0.04 μg/L, respectively, and in porewater it was 2.71 ± 0.49 μg/L, 1.50 ± 0.29 μg/L and 1.81 ± 0.28 μg/L, respectively. The average concentrations of NP in DGT were 0.23 ± 0.03 μg/L, 0.08 ± 0.02 μg/L, and 0.10 ± 0.02 μg/L, respectively, and in porewater 2.21 ± 0.37 μg/L, 1.48 ± 0.33 μg/L, and 1.73 ± 0.30 μg/L, respectively. It was worth noting that BPA concentrations in porewater and DGT were slightly higher than those of NP. This may be attributed to the higher accumulation of NP in sediments, which resulted in a larger pool of releasable NP for diffusion from sediments into porewater, leading to a residual NP concentrations in porewater close to that of BPA, similar to the results in other studies (Zhang et al., 2009, 2011). In addition, this result was further supported by the distribution coefficient ($K_d$), which ranged from 3.07 to 19.48 g/mL for NP across the three zones, while for BPA,

the $K_d$ values ranged from 0.71 to 4.53 g/mL, with an average value approximately 4.19 times lower than that of NP (Table S2).

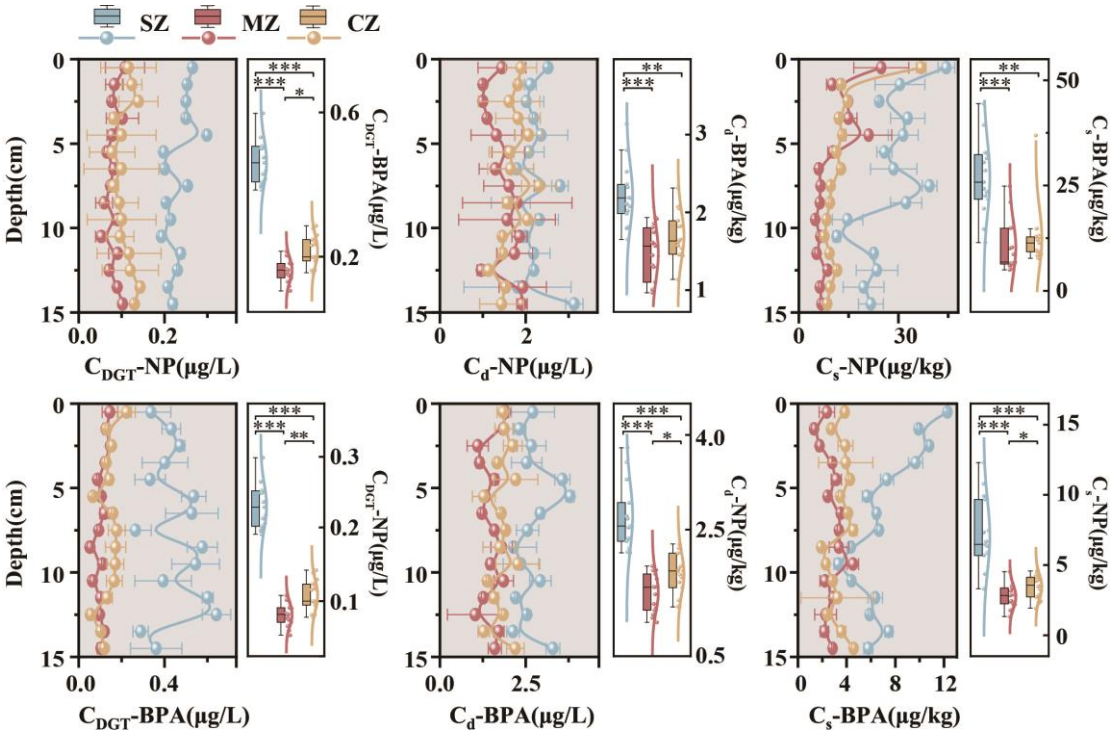


**Fig.2** Variation of NP and BPA concentrations in DGT, porewater and sediment profiles of the SZ, MZ and CZ. Here, "*", "**" and "***" indicate $p < 0.05$, 0.01 and 0.001, respectively.

### 3.3 BPA and NP diffusion in sediment with depth from different zones

Fig. S6 shows the profile variations for the $R$ values with depth in the SZ, MZ and CZ. For BPA, the $R$ values ranged from 0.093 to 0.272 in the SZ, 0.029 to 0.134 in the MZ, and 0.029 to 0.121 in the CZ, with mean values of 0.171 ± 0.058, 0.075 ± 0.026 and 0.080 ± 0.024, respectively. For NP, the $R$ values ranged from 0.070 to 0.127 in the SZ, 0.028 to 0.092 in the MZ, and 0.035 to 0.106 in the CZ, with mean values of 0.107 ± 0.015, 0.059 ± 0.018 and 0.062 ± 0.020, respectively. The $R$ for BPA was higher than NP in all three zones due to the higher hydrophilicity and lower p$K_a$ (9.6) of BPA.

Furthermore, in the SZ, *R* values of BPA and NP were mostly greater than 0.1, indicating there was a partial resupply from sediment to porewater, but that this resupply was insufficient to maintain initial porewater concentrations. However, in the MZ and the CZ, *R* values of BPA and NP were mostly below 0.1, indicating limited resupply from sediment to porewater (Chen et al., 2014).

### 3.4 Differences in microbial communities of the sediments from the three zones

The bacterial community composition of the CZ was shown to be different to the SZ and the MZ based on the Bray-Curtis, the CZ samples were distinctly separated from the SZ and the MZ on the pCo1 (Fig. 3a). Similarly, the Shannon and Chao1 indices for the CZ were significantly lower than for the SZ and the MZ ($p$<0.001), indicating the diversity of the microbial community of the CZ was the lowest (Fig. 3b). *Proteobacteria* were the most dominant phyla in all zones: SZ 28.68 ± 3.35%, MZ 31.07 ± 4.18%, and CZ 76.34 ± 0.63%. *Desulfobacterota* and *Bacteroidota* were also the main phyla in the SZ: 16.68 ± 1.56%, and 9.84 ± 1.56 %, respectively, and the MZ: 18.69 ± 2.68%, and 11.81 ± 2.48%, respectively (Fig. 3c). Additionally, among the top 20 genera in the three zones (Fig. 3c and Fig. S7), *Woeseia* (8.84 ± 0.16%) and *Subgroup 23* (3.19 ± 0.92%) showed the highest relative abundance in the SZ, *Sva1033* (7.80 ± 2.9 %) showed the highest relative abundance in the MZ, and *Vibrio* (67.00 ± 0.79%) and *Halarcobacter* (5.02 ± 1.80 %) showed the highest relative abundance in the CZ. Based on statistical analysis of metagenomic profiles (Fig. 3d-f), among the top 20 genera in these three zones, *B2M28*, *BD2-11_terrestrial_group*, *Subgroup 23* and

448 *SBR1031* were significantly higher in the SZ ($p$<0.05). *Sva1033*, *Halioglobus* and
449 *Lutimonas* were significantly higher in the MZ ($p$<0.05), and *Vibrio*, *Halarcobacter*,
450 *Clostridiisalibacter and Marinobacterium* were significantly higher in the CZ
451 ($p$<0.001). Fig. 3g shows the BPA and NP potential biotransformation pathways and the
452 related functional gene abundances based on the KEGG pathway database and previous
453 studies (Yu et al., 2019; Wu et al., 2022). The relative abundance of most functional
454 genes for both BPA and NP (such as *alkB* and *pobA* etc.) were significantly higher in
455 the MZ ($p$<0.05). Furthermore, the relative abundance of the bisphenol degradation
456 (ko00363) pathway was also significantly higher in the MZ ($p$<0.05).
457 Microbial interactions in the three zones was also examined by establishing co-
458 occurrence networks of the SZ (Fig. S8a), MZ (Fig. S8b) and CZ (Fig. S8c).
459 *Proteobacteria* were shown to be the main phyla in the SZ, MZ and CZ. The MZ
460 network captured more nodes (175), edges (788), and higher average clustering
461 coefficient (0.468) than either the SZ network (170, 782, and 0.395) or the CZ network
462 (171, 788, and 0.393), indicating higher species co-occurrence association frequencies
463 in the MZ. Additionally, the positive/negative edge ratios in the SZ and CZ networks
464 were lower than in the MZ network, suggesting stronger species competition in the
465 oxygen-limited SZ and CZ (Lei et al., 2023). In contrast to the SZ and CZ networks,
466 the MZ network showed higher modular structures (Modularity>0.4) indicating non-
467 random MZ network structures which were unlikely to appear due to chance (Zhao et
468 al., 2023). Additionally, 14 key ASVs were identified as “connectors” in the MZ

network, compared to 10 in the SZ and CZ networks.

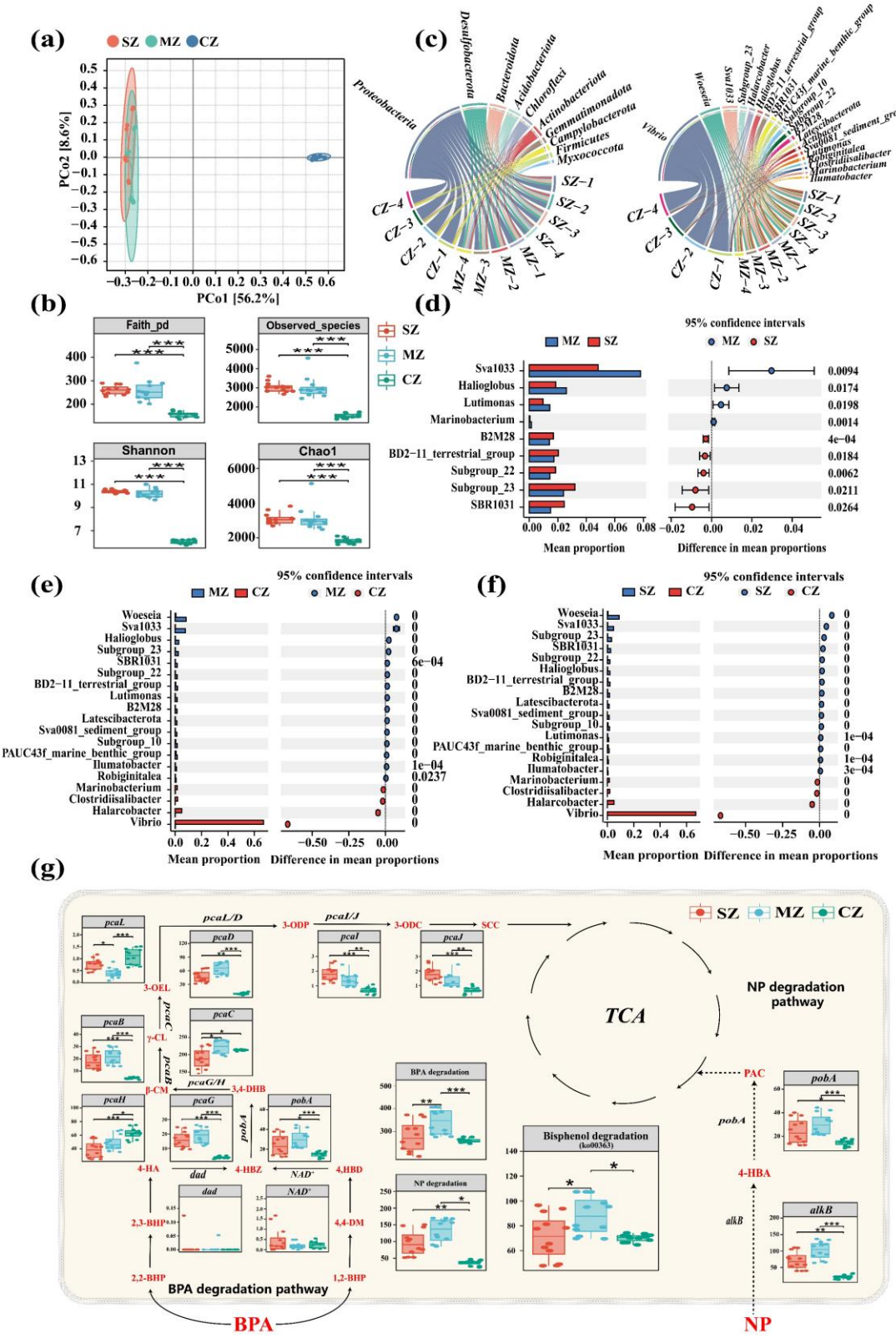


**Fig. 3** Differences in microbial communities in the different estuarine zones: (a) the PCoA plot based on the Bray-Curtis, (b) boxplots showing the bacterial alpha diversity

473 indices in sediments, (c) Chord maps of the top 10 phyla and top 20 genera, in which -
474 1, -2, -3 and -4 correspond to part 1, part 2, part 3, part 4 of the sediment profiles in the
475 SZ and the MZ as mentioned in section 2.5. Differential analysis of the top 20 genera
476 between (d) the SZ and the MZ, (e) the MZ and the CZ and (f) the SZ and the CZ by
477 STAMP (Statistical Analysis of Metagenomic Profiles), and (g) possible bio-
478 transformation pathways of BPA and NP (the abbreviations of intermediates involved
479 in the pathways are listed in Table S3). "*", "**" and "***" indicate $p < 0.05$, 0.01 and
480 0.001, respectively.

481 **4. Discussion**

482 **4.1 Seawater incursion reshapes the environmental spatial gradient in estuarine**
483 **sediments**

484 In SZ sediments (slight seawater incursion), the environmental conditions were
485 relatively stable and anoxic with $O_2$ supplied exclusively by diffusion across the
486 sediment surface (Fig. 4) (Huettel et al., 2018). Here, the $O_2$ supply was insufficient to
487 support bioremediation and respiration of heterotrophic microorganisms, resulting in
488 rapid anoxia in surface layer sediments of the SZ (Meng et al., 2022). Subsequently, the
489 intense hypoxic respiration of microorganisms in the SZ led to the consumption of TOC
490 as a carbon source (van Erk et al., 2023), resulting in the low observed TOC
491 concentrations here. However, with the increase in seawater incursion, the
492 environmental conditions changed significantly (Fig. 1 and S4). Tidal pumping and
493 advection transport of oxygenated seawater enhanced gas exchange rates in MZ

494 sediments with moderate seawater incursion, increasing $O_2$ penetration and reducing
495 $CO_2$ accumulation (Huettel et al., 2018; Karthikeyan et al., 2020), shifting these
496 sediments to relatively oxic conditions. For CZ sediments i.e., permanently inundated
497 by seawater, the exchange between oxygenated seawater and porewater can only
498 influence the surface layer of sediments, resulting in anoxic conditions at the bottom
499 (Geng et al., 2022). Furthermore, and in contrast to the SZ, frequent oxygenated
500 seawater level fluctuations in the MZ and CZ induced oxidative stress from reactive
501 oxygen species, which inhibited microbial respiration and facilitated the accumulation
502 of TOC (van Erk et al., 2023). Hence, the TOC was significantly higher in the MZ and
503 the CZ than the SZ ($p$<0.05), and there was no statistical difference between the MZ
504 and the CZ ($p$>0.28) (Fig. S5). Salinity and pH, as the environmental tracers of seawater
505 incursion (Zhao et al., 2023), were also different amongst the three estuarine zones (Fig.
506 1). Since seawater incursion began at the bottom (He et al., 2021), the sediments at the
507 bottom of the estuarine SZ, MZ and CZ all had higher salinity and lower pH . As the
508 degree of seawater incursion increased, the pH in the sediments continued to decrease
509 and the salinity continued to increase. This resulted in the CZ, with complete seawater
510 incursion, showing the lowest pH ($p$<0.001) and the highest salinity ($p$<0.05) of all
511 three zones. In summary, seawater incursion changed the spatial gradient of the
512 dissolved oxygen environment, TOC ($p$<0.05), pH ($p$<0.001) and salinity ($p$<0.05)
513 significantly, and it will further drive changes in the distribution and diffusion BPA and
514 NP in sediments.

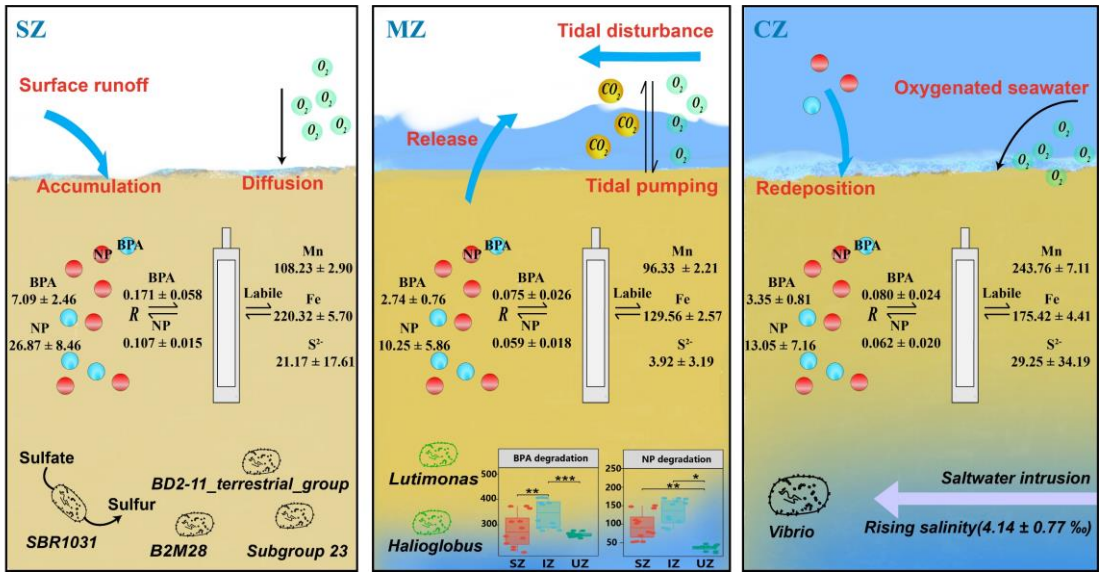


**Fig. 4** Biogeochemical processes at the IESW in the different estuarine zones under seawater incursion. BPA and NP concentrations in μg/kg (leftmost in each figure); Mn and Fe concentrations in μg/L, $S^{2-}$ concentrations in mg/L (rightmost in each figure).

### 4.2 Seawater incursion enhances the mobility of BPA and NP in sediments

Commonly, sediments with higher TOC content should have a stronger ability to trap pollutants (Xu et al., 2018), however seawater incursion alters this pattern, and the distribution of organic pollutants in sediments is dominated by hydrodynamic conditions (Ma et al., 2023) (Fig. 4). Frequent tidal action in the MZ facilitated material exchange between sediment and overlying seawater, resulting in the release of more BPA and NP into the seawater (Liu et al., 2022b). In addition, the oxygenated environment of the MZ, generated by tidal water level fluctuations, promoted the bio-transformation of BPA and NP (Huettel et al., 2018; Karthikeyan et al., 2020; Liu et al., 2022b). Moreover, dilution by open seawater is an important factor influencing the concentrations and spatial distribution of pollutants (Cao et al., 2024). Seawater

530 incursion leads to a large influx of seawater, which further dilutes the concentrations of
531 target substances (Van Ael et al., 2013; Wu et al., 2014; Wang et al., 2019a). As a result,
532 the lowest concentrations of BPA and NP were observed in the MZ (Fig. 2). As for the
533 CZ, with complete seawater inundation, the sedimentary environment has become
534 relatively stable after undergoing a similar process to that of the MZ. Suspended
535 sediment particles transported from the MZ by tidal events gradually settle in the CZ.
536 BPA and NP still adsorbed on these suspended particles will accumulate in the CZ as
537 these particles are deposited. However, due to the very slow deposition process
538 (Álvarez-Iglesias et al., 2007), the concentration of BPA and NP in the CZ and the MZ
539 sediments did not change much. Meanwhile, in the estuarine SZ, TOC had a great
540 dominance of pollutants due to less influence from seawater incursion, which promoted
541 the accumulation of BPA and NP in sediments. Additionally, the diffusion and
542 distribution of BPA and NP in DGT and porewater are shown in Fig. 4. Higher TOC in
543 the MZ and CZ sediments provided more adsorption sites for binding BPA and NP (Xu
544 et al., 2018). Meanwhile, in the MZ and CZ, the "salting-out" effect induced by high
545 salinity promoted the separation of BPA and NP from the water, combined with higher
546 $P_c$ (Table S2), both of them hindering the diffusion of these compounds. All of these
547 factors significantly decreased resupply in the MZ and CZ, and resulted in the highest
548 $R$ in the SZ ($p$<0.001) (Fig. S9). DGT concentrations reflected the labile fractions of
549 target substances in sediments and, similarly to porewater, they both depended on the
550 resupply capacity and target substance concentrations from the sediments (Arsic et al.,

2018). Thus, the highest *R* and highest concentrations of BPA and NP in sediments ($p$<0.01) also determined their highest DGT ($p$<0.001) and porewater concentrations in SZ ($p$<0.01).

### 4.3 Microbial community differences and their potential correlation with BPA and NP under seawater incursion

The SZ sediments, with slight seawater coverage, were characterized by high relative abundances of *B2M28*, *BD2-11_terrestrial_group*, *Subgroup 23* and *SBR1031*. *B2M28* and *BD2-11_terrestrial_group* are typically found with high relative abundances in polluted areas (Quintero et al., 2022; Wang et al., 2024b), *Subgroup 23* is commonly found in anoxic environments (Walker et al., 2023), and *SBR1031* is a common sulfate-reducing bacteria (Zhang et al., 2023b) (Fig. 3). This information provides further evidence that the SZ with anoxic deposition environments (high $S^{2-}$ concentrations) accumulated the highest levels of BPA and NP. Meanwhile, seawater incursion drove the evolution of microbial communities, and significantly changed them to adapt to the reshaped environmental conditions (Fig. 4). In the moderate seawater incursion sediments of the MZ, *Halioglobus* (with potential for contribution to hydrocarbon degradation (Suárez-Moo et al., 2020)) and *Lutimonas* (a strictly aerobic genus (Ma et al., 2015)) showed significantly higher relative abundance than in the SZ and CZ ($p$<0.05). Additionally, *Bacteroidota*, as one of the main phyla in the sediments of all three zones, which included heterotrophic bacteria capable of degrading organic compounds, also showed the highest relative abundance in the MZ (Savvichev et al.,

572 2023). These indicate that the MZ with oxic conditions seemed to exhibit stronger
573 degradation of organic matter. This is consistent with the results shown in section 3.4
574 (Fig. 3g) i.e., that the most functional genes related to the biotransformation of BPA and
575 NP were significantly higher in the MZ ($p$<0.05). Seawater incursion created the oxic
576 conditions of the MZ, which appeared to favor increased biotransformation of BPA and
577 NP, and explains the observation that the lowest concentrations of BPA and NP were in
578 this zone. Once seawater coverage was complete, the composition of the microbial
579 community would be further modified due to the shift in environmental conditions.
580 Salinity, which was highest in the CZ with full seawater incursion, has been shown to
581 be a robust predictor for microbial community distribution in estuarine sediments.
582 Previous studies have also shown that high salinity would inhibit the diversity and
583 functioning of microbial communities, and result in the dominance of *Proteobacteria*
584 (Zhang et al., 2017). Thus, the highest salinity observed in the CZ shaped the lowest
585 diversity in the microbial community ($p$<0.001), and the abnormal dominance of
586 *Proteobacteria* (76.34 ± 0.63%) (Fig. 3). Moreover, the significantly higher relative
587 abundance genera of *Vibrio*, *Clostridiisalibacter*, *Halarcobacter* and *Marinobacterium*
588 in the CZ are commonly observed in high salinity marine sediments (Sun et al., 2015;
589 Wang et al., 2019b; Baek et al., 2021; Romanenko et al., 2022). Taken together, these
590 findings suggest that complete seawater incursion has severely affected the microbial
591 composition of CZ sediments. Indeed, the microbial community structure in the CZ was
592 unlikely to appear just by chance, and seems to be controlled by seawater incursion,

593 which corresponds with the higher observed modular structure (Modularity>0.4) of the
594 microbial co-occurrence networks in the CZ (Fig. S8). Meanwhile, the relative
595 abundance of biotransformation genes related to BPA and NP were significantly
596 reduced ($p$<0.05), and may be attributed to the degradation of these pollutants typically
597 performed under oxic conditions. Thus, the biodegradation of BPA and NP appears to
598 cease in the CZ.

599 **4.4 Evaluation of possible EDC release from estuarine sediments due to sea level**
600 **rise**

601 Coastal estuaries provide crucial ecological and economic functions, including
602 carbon sequestration, support for fisheries and water quality improvement, creating
603 economic services valued at up to US$194,000 $ha^{-1}y^{-1}$ (Costanza et al., 2014). However,
604 with global sea level rise, coastal wetlands will be affected, and the threat to aquatic
605 organisms in the ocean will continue to increase due to the transportation and
606 transformation of pollutants (Irrgang et al., 2022). Based on the median of three
607 greenhouse gas concentration scenarios (RCP26, RCP45, and RCP85), sea level rise is
608 projected to be 39.3 cm, 52.9 cm, and 84.6 cm by 2100 (Mengel et al., 2016). Further,
609 under business-as-usual human adaptation scenarios i.e., population density of 5–20
610 people $km^{-2}$, coastal wetland areas would be lost by up to 8%, 12%, and 30% for RCP26,
611 RCP45, and RCP85 by 2100, respectively (Schuerch et al., 2018). Consequently, under
612 these three scenarios, the cumulative additional release of BPA and NP between 2024
613 and 2100 is projected to be 0.6 t, 0.8 t and 1.8 t, and 0.5 t, 0.7 t and 1.5 t, respectively,

614 from Red Beach, based on the established model (Fig. 5). Due to the environmental
615 persistence and bioaccumulation of BPA and NP, they would be accumulated and
616 concentrated in marine species, such as mollusks, crustaceans, mussels, and fish
617 (Arditsoglou and Voutsa, 2012) leading to marked anomalies in growth and
618 reproductive rates and migration. This raises concerns for the health and sustainability
619 of estuarine ecosystems, requiring more attention from government and communities
620 and demonstrating the need for advanced management strategies. Increasing vegetative
621 cover in estuarine wetlands could be a viable management strategy since it could
622 decrease sediment suspension under hydraulic disturbance, reducing the risk of
623 pollutant mobilization (Reif et al., 2022). Meanwhile, more rigorous monitoring
624 campaigns should be conducted to assess the mobility and risk of contaminants (Bavi
625 et al., 2023). Additionally, there is a need to develop more stringent chemical
626 management policies, and encourage the use of eco-friendly products to prevent the
627 release of contaminants into coastal estuaries (Pastorino et al., 2024).

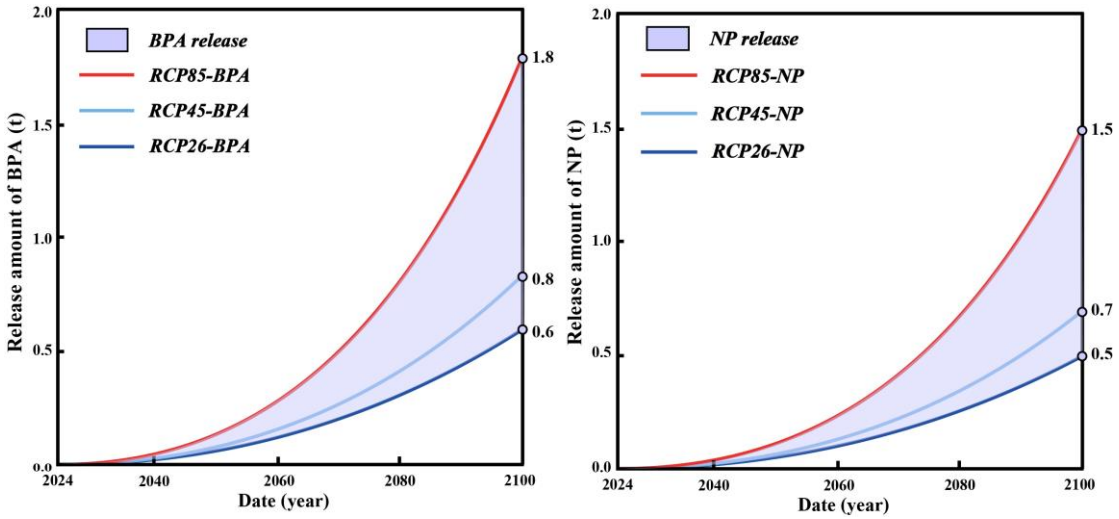


628

629 **Fig. 5** Cumulative additional release predictions of (a) BPA and (b) NP under three

630 Representative Concentration Pathways (RCP26, RCP45 and RCP85) between 2024
631 and 2100.

632 **5. Conclusions**

633 This study reveals continuing seawater incursion has significantly altered
634 geochemical processes and microbial communities of estuarine sediments, which in
635 turn has shifted the distribution, diffusion and biotransformation of EDCs in the Red
636 Beach wetland of the Liaohe estuary. Specifically, the intense tidal actions in the MZ
637 with moderate seawater incursion, resulted in the release of BPA and NP from sediments
638 to overlying seawater. Further, the oxic environment of MZ sediments caused by tidal
639 actions enhanced the potential for BPA and NP biotransformation. These factors
640 contributed to the lowest BPA and NP concentrations observed in our study. However,
641 in the CZ, with complete seawater inundation hence highest observed salinity and
642 lowest pH, the diversity of the microbial community was significantly reduced
643 ($p$<0.001) and dominated by *Proteobacteria* (76.34 ± 0.63%). The biodegradation of
644 BPA and NP is significantly reduced and, indeed, tended to stop altogether. This
645 facilitates the continued deposition and accumulation of BPA and NP from the water
646 body into the CZ sediment, turning it into an important sink and source of EDCs. As
647 for the SZ, with slight seawater incursion, the relatively stable anoxic sedimentary
648 environment resulted in the lowest TOC concentrations, highest BPA and NP
649 concentrations, and the strongest resupply capacity. The release of BPA and NP from
650 the Red Beach wetlands could reach a maximum of 1.8 t and 1.5 t, respectively, by 2100

due to seawater incursion, calling for government attention.

However, there are still many shortcomings and limitations in this study. The next study could expand the study area in the estuary and increase the sampling frequency to further elucidate the spatial and temporal patterns of the influence of seawater incursion on the fate of EDCs in the estuarine environment. In addition, simulation experiments in laboratory by controlling environmental conditions such as salinity gradients and tidal cycles should be carried out to provide a more valuable theoretical basis for the migration and transformation of EDCs in estuarine sedimentary environments under the influence of seawater incursion. Meanwhile, based on more abundant field survey and *in situ* experimental data, the biogeochemical processes and mechanisms of EDCs in estuarine environments under the influence of seawater incursion should be further deduced with the help of artificial intelligence methods such as machine learning. In addition, the impact of seawater incursion on the fate of other emerging organic pollutants (e.g., antimicrobials, perfluorinated compounds, and tyre leaching chemicals) should also be investigated. These studies will help to improve the data and theories on the fate, transport, transformation and risk of emerging organic pollutants in estuaries, and provide a technical basis for the development of coastal ecological and economic restoration strategies.

**Acknowledgments**

This research was financially supported by the National Natural Science Foundation of

China (Grant no. 41977325), and the Projects of International Cooperation and Exchange of the National Natural Science Foundation of China (Grant No. 42211530483).

**References**

Álvarez-Iglesias, P., Quintana, B., Rubio, B., Pérez-Arlucea, M., 2007. Sedimentation rates and trace metal input history in intertidal sediments from San Simón Bay (Ría de Vigo, NW Spain) derived from 210Pb and 137Cs chronology. J. Environ. Radioact. 98, 229–250. https://doi.org/10.1016/j.jenvrad.2007.05.001

Anschutz, P., Smith, T., Mouret, A., Deborde, J., Bujan, S., Poirier, D., Lecroart, P., 2009. Tidal sands as biogeochemical reactors. Estuar. Coast. Shelf Sci. 84, 84–90. https://doi.org/10.1016/j.ecss.2009.06.015

Arditsoglou, A., Voutsa, D., 2012. Occurrence and partitioning of endocrine-disrupting compounds in the marine environment of Thermaikos Gulf, Northern Aegean Sea, Greece. Mar. Pollut. Bull. 64, 2443–2452. https://doi.org/10.1016/j.marpolbul.2012.07.048

Arsic, M., Teasdale, P.R., Welsh, D.T., Johnston, S.G., Burton, E.D., Hockmann, K., Bennett, W.W., 2018. Diffusive Gradients in Thin Films Reveals Differences in Antimony and Arsenic Mobility in a Contaminated Wetland Sediment during an Oxic-Anoxic Transition. Environ. Sci. Technol. 52, 1118–1127. https://doi.org/10.1021/acs.est.7b03882

Baek, J., Jeong, J., Kim, J.-H., Sukhoom, A., Kim, W., 2021. Halarcobacter arenosus

694 sp. nov., isolated from marine sediment. Arch. Microbiol. 203, 817–822.
695 https://doi.org/10.1007/s00203-020-02075-8
696 Bavi, H., Gharaie, M.H.M., Moussavi-Harami, R., Zand-Moghadam, H., Mahboubi, A.,
697 Tohidi, M.R., 2023. Spatial dispersion hot spots of contamination and human
698 health risk assessments of PTEs in surface sediments of streams around porphyry
699 copper mine, Iran. Environ. Geochem. Health 45, 3907–3931.
700 https://doi.org/10.1007/s10653-022-01471-x
701 Bradley, P.M., Battaglin, W.A., Iwanowicz, L.R., Clark, J.M., Journey, C.A., 2016.
702 Aerobic biodegradation potential of endocrine-disrupting chemicals in surface-
703 water sediment at Rocky Mountain National Park, USA. Environ. Toxicol. Chem.
704 35, 1087–1096. https://doi.org/10.1002/etc.3266
705 Cao, Y., Wang, J., Xin, M., Wang, B., Lin, C., 2024. Spatial distribution and partition
706 of polycyclic aromatic hydrocarbons (PAHs) in the water and sediment of the
707 southern Bohai Sea: Yellow River and PAH property influences. Water Res. 248,
708 120873. https://doi.org/10.1016/j.watres.2023.120873
709 Chakraborty, P., Jayachandran, S., Lekshmy, J., Padalkar, P., Sitlhou, L., Chennuri, K.,
710 Shetye, S., Sardar, A., Khandeparker, R., 2019. Seawater intrusion and
711 resuspension of surface sediment control mercury (Hg) distribution and its
712 bioavailability in water column of a monsoonal estuarine system. Sci. Total
713 Environ. 660, 1441–1448. https://doi.org/10.1016/j.scitotenv.2018.12.477
714 Chen, C.-E., Jones, K.C., Ying, G.-G., Zhang, H., 2014. Desorption Kinetics of

715 Sulfonamide and Trimethoprim Antibiotics in Soils Assessed with Diffusive
716 Gradients in Thin-Films. Environ. Sci. Technol. 48, 5530–5536.
717 https://doi.org/10.1021/es500194f
718 Chen, J., Zhang, B., Wang, C., Wang, P., Cui, G., Gao, H., Feng, B., Zhang, J., 2024.
719 Insight into the enhancement effect of humic acid on microbial degradation of
720 triclosan in anaerobic sediments. J. Hazard. Mater. 461, 132549.
721 https://doi.org/10.1016/j.jhazmat.2023.132549
722 Chen, Q., Lan, Y., Shi, J., Liu, W., Zhu, B., Sun, D., Duan, S., 2019. Levels of NP and
723 BPA in the Pearl River Estuary, China: Fluctuations with Country Policy Changes
724 over the Past 40 Years. Int. J. Environ. Res. Public. Health 16, 4100.
725 https://doi.org/10.3390/ijerph16214100
726 Chen, X., Hu, Z., Xie, H., Zhang, J., Liang, S., Wu, H., Zhuang, L., 2022. Priming
727 effects of root exudates on the source-sink stability of benzo[*a*]pyrene in wetlands:
728 A microcosm experiment. J. Hazard. Mater. 429, 128364.
729 https://doi.org/10.1016/j.jhazmat.2022.128364
730 Chiriac, F.L., Pirvu, F., Paun, I., 2021. Investigation of endocrine disruptor pollutants
731 and their metabolites along the Romanian Black Sea Coast: Occurrence,
732 distribution and risk assessment. Environ. Toxicol. Pharmacol. 86, 103673.
733 https://doi.org/10.1016/j.etap.2021.103673
734 Costanza, R., de Groot, R., Sutton, P., van der Ploeg, S., Anderson, S.J., Kubiszewski,
735 I., Farber, S., Turner, R.K., 2014. Changes in the global value of ecosystem

services. Glob. Environ. Change 26, 152–158. https://doi.org/10.1016/j.gloenvcha.2014.04.002

De Weert, J., Viñas, M., Grotenhuis, T., Rijnaarts, H., Langenhoff, A., 2010. Aerobic nonylphenol degradation and nitro-nonylphenol formation by microbial cultures from sediments. Appl. Microbiol. Biotechnol. 86, 761–771. https://doi.org/10.1007/s00253-009-2394-9

Diao, P., Chen, Q., Wang, R., Sun, D., Cai, Z., Wu, H., Duan, S., 2017. Phenolic endocrine-disrupting compounds in the Pearl River Estuary: Occurrence, bioaccumulation and risk assessment. Sci. Total Environ. 584–585, 1100–1107. https://doi.org/10.1016/j.scitotenv.2017.01.169

Dong, L., Liu, Z., Xin, Z., Song, C., Bai, X., Li, J., Zhang, Y., Valverde-Pérez, B., Zhang, C., 2024. Runoff variation alters estuarine sediment microbiome and nitrogen removal processes by affecting salinity. Sci. Total Environ. 955, 176880. https://doi.org/10.1016/j.scitotenv.2024.176880

Du, L., Guo, W., Zhang, X., Yue, J., Li, D., Li, J., Baeyens, W., Gao, Y., 2025. Fate of bisphenol A and nonylphenol in the lake riparian zone: Distribution, transport, and microbial response. J. Hazard. Mater. 483, 136662. https://doi.org/10.1016/j.jhazmat.2024.136662

Du, L., Wang, S., Jiang, X., Wu, Z., Bratkic, A., Guo, W., 2024. Water depth alters the fate of estrone across the sediment–water interface in a typical inland lake. J. Hydrol. 645, 132184. https://doi.org/10.1016/j.jhydrol.2024.132184

Fetters, K.J., Costello, D.M., Hammerschmidt, C.R., Burton Jr., G.A., 2016. Toxicological effects of short-term resuspension of metal-contaminated freshwater and marine sediments. Environ. Toxicol. Chem. 35, 676–686. https://doi.org/10.1002/etc.3225

Gao, L., Yan, C., Yang, C., Li, R., Wu, Q., Tian, D., Ouyang, L., 2025. Salty tide enhanced ecotoxicological risk of trace metals in the lower reach of the Pearl River, China via altering their phase partitioning and chemical speciation. J. Hydrol. 653, 132761. https://doi.org/10.1016/j.jhydrol.2025.132761

Gao, Y., Liang, T., Tian, S., Wang, L., Holm, P.E., Bruun Hansen, H.C., 2016. High-resolution imaging of labile phosphorus and its relationship with iron redox state in lake sediments. Environ. Pollut. 219, 466–474. https://doi.org/10.1016/j.envpol.2016.05.053

Geng, X., Barker, C.H., MacFadyen, A., Boufadel, M.C., Lee, K., Thrift-Viveros, D.L., Jones, R., O'Connor, C., 2022. Oil biodegradation in permeable marine sediments: Effects of benthic pore-water advection and solute exchange. J. Hazard. Mater. 436, 129211. https://doi.org/10.1016/j.jhazmat.2022.129211

Gong, X., Chen, Z., Deng, Y., Zhao, D., Gao, P., Zhang, L., Tu, Q., Qu, L., Zheng, L., Zhang, Y., Song, C., Liu, J., 2022. Contrasting archaeal and bacterial community assembly processes and the importance of rare taxa along a depth gradient in shallow coastal sediments. Sci. Total Environ. 852, 158411. https://doi.org/10.1016/j.scitotenv.2022.158411

778 Gu, S., Yin, J., Shang, M., Ke, H., Dong, J., Zhu, X., Xie, H., 2024. Transport, sources,
779 and risks of particulate antibiotics in coastal environments: The crucial role of
780 particles in mud coasts. Mar. Pollut. Bull. 209, 117204.
781 https://doi.org/10.1016/j.marpolbul.2024.117204
782 Guo, Q., Zhao, Y., Li, M., Liu, J., 2022. Radium isotope assessment of submarine
783 groundwater discharge and associated nutrient inputs in Eastern Liaodong Bay,
784 China. Front. Mar. Sci. 9. https://doi.org/10.3389/fmars.2022.916109
785 He, W., Jiang, A., Zhang, J., Xu, H., Xiao, Y., Chen, S., Yu, X., 2021. Hydrodynamic
786 characteristics of lateral withdrawal in a tidal river channel with saltwater intrusion.
787 Ocean Eng. 228, 108905. https://doi.org/10.1016/j.oceaneng.2021.108905
788 He, W., Li, J., Chen, M., Sun, H., Zhang, L., Lu, Y., Jia, Y., Zhang, H., 2023. A
789 mathematical model to simulate the release of Fe and Mn from sediments in a
790 drinking water reservoir. Environ. Res. 238, 117232.
791 https://doi.org/10.1016/j.envres.2023.117232
792 Hlaing, N.O., Azhikodan, G., Yokoyama, K., 2024. Effect of monsoonal rainfall and
793 tides on salinity intrusion and mixing dynamics in a macrotidal estuary. Mar.
794 Environ. Res. 202, 106791. https://doi.org/10.1016/j.marenvres.2024.106791
795 Hu, Z., Guo, K., Yang, Y., Zhang, M., 2023. Field survey and analysis of water flux and
796 salinity gradients considering the effects of sea ice coverage and rubber dam: a
797 case study of the Liao River Estuary, China. Front. Mar. Sci. 10.
798 https://doi.org/10.3389/fmars.2023.1154150

799 Huang, Y.-F., Wang, P.-W., Huang, L.-W., Lai, C.-H., Yang, W., Wu, K.-Y., Lu, C.A.,
800 Chen, H.-C., Chen, M.-L., 2017. Prenatal Nonylphenol and Bisphenol A
801 Exposures and Inflammation Are Determinants of Oxidative/Nitrative Stress: A
802 Taiwanese Cohort Study. Environ. Sci. Technol. 51, 6422–6429.
803 https://doi.org/10.1021/acs.est.7b00801
804 Huang, Y.-F., Wang, P.-W., Huang, L.-W., Lin, M.-H., Yang, W., Chen, H.-C., Yu, K.-
805 P., Chen, M.-L., 2018. Interactive effects of nonylphenol and bisphenol A exposure
806 with oxidative stress on fetal reproductive indices. Environ. Res. 167, 567–574.
807 https://doi.org/10.1016/j.envres.2018.08.007
808 Huettel, M., Overholt, W.A., Kostka, J.E., Hagan, C., Kaba, J., Wells, Wm.B., Dudley,
809 S., 2018. Degradation of Deepwater Horizon oil buried in a Florida beach
810 influenced by tidal pumping. Mar. Pollut. Bull. 126, 488–500.
811 https://doi.org/10.1016/j.marpolbul.2017.10.061
812 Huludao Environmental Quality Report, 2024. Huludao Ecological Environment
813 Bureau. https://sthj.hld.gov.cn/zwgk/zfxxgk/fdzdgknr/tjxx/
814 Irrgang, A.M., Bendixen, M., Farquharson, L.M., Baranskaya, A.V., Erikson, L.H.,
815 Gibbs, A.E., Ogorodov, S.A., Overduin, P.P., Lantuit, H., Grigoriev, M.N., Jones,
816 B.M., 2022. Drivers, dynamics and impacts of changing Arctic coasts. Nat. Rev.
817 Earth Environ. 3, 39–54. https://doi.org/10.1038/s43017-021-00232-1
818 Ji, X., Challis, J.K., Cantin, J., Cardenas Perez, A.S., Gong, Y., Giesy, J.P., Brinkmann,
819 M., 2022. A novel passive sampling and sequential extraction approach to

investigate desorption kinetics of emerging organic contaminants at the sediment−water interface. Water Res. 217, 118455. https://doi.org/10.1016/j.watres.2022.118455

Karthikeyan, S., Kim, M., Heritier-Robbins, P., Hatt, J.K., Spain, J.C., Overholt, W.A., Huettel, M., Kostka, J.E., Konstantinidis, K.T., 2020. Integrated Omics Elucidate the Mechanisms Driving the Rapid Biodegradation of Deepwater Horizon Oil in Intertidal Sediments Undergoing Oxic–Anoxic Cycles. Environ. Sci. Technol. 54, 10088–10099. https://doi.org/10.1021/acs.est.0c02834

Kirwan, M.L., Megonigal, J.P., 2013. Tidal wetland stability in the face of human impacts and sea-level rise. Nature 504, 53–60. https://doi.org/10.1038/nature12856

Lee, C.-C., Hsieh, C.-Y., Chen, C.S., Tien, C.-J., 2020. Emergent contaminants in sediments and fishes from the Tamsui River (Taiwan): Their spatial-temporal distribution and risk to aquatic ecosystems and human health. Environ. Pollut. 258, 113733. https://doi.org/10.1016/j.envpol.2019.113733

Lee, C.-C., Jiang, L.-Y., Kuo, Y.-L., Hsieh, C.-Y., Chen, C.S., Tien, C.-J., 2013. The potential role of water quality parameters on occurrence of nonylphenol and bisphenol A and identification of their discharge sources in the river ecosystems. Chemosphere 91, 904–911. https://doi.org/10.1016/j.chemosphere.2013.02.006

Lee, J., Biemond, B., de Swart, H., Dijkstra, H.A., 2024. Increasing risks of extreme salt intrusion events across European estuaries in a warming climate. Commun.

841 Earth Environ. 5, 1–7. https://doi.org/10.1038/s43247-024-01225-w
842 Lei, S., Wang, X., Wang, J., Zhang, L., Liao, L., Liu, G., Wang, G., Song, Z., Zhang,
843 C., 2023. Effect of aridity on the β-diversity of alpine soil potential diazotrophs:
844 insights into community assembly and co-occurrence patterns. mSystems 9,
845 e01042-23. https://doi.org/10.1128/msystems.01042-23
846 Li, C., Ding, S., Chen, M., Zhong, Z., Sun, Q., Wang, Y., 2023a. Visualizing
847 biogeochemical heterogeneity in soils and sediments: A review of advanced micro-
848 scale sampling and imaging methods. Crit. Rev. Environ. Sci. Technol. 53, 1229–
849 1253. https://doi.org/10.1080/10643389.2022.2128239
850 Li, W., Li, Q., Pan, Z., Burgaud, G., Ma, H., Zheng, Y., Wang, M., Cai, L., 2023b.
851 Seasonal and Spatial Dynamics of Fungal Diversity and Communities in the
852 Intertidal Zones of Qingdao, China. J. Fungi 9, 1015.
853 https://doi.org/10.3390/jof9101015
854 Li, Y., Han, C., Luo, J., Jones, K.C., Zhang, H., 2021. Use of the Dynamic Technique
855 DGT to Determine the Labile Pool Size and Kinetic Resupply of Pesticides in Soils
856 and Sediments. Environ. Sci. Technol. 55, 9591–9600.
857 https://doi.org/10.1021/acs.est.1c01354
858 Liang, Y., Li, H., Li, S., Chen, S., 2023. Organic diffusive gradients in thin films (o-
859 DGT) for determining environmental behaviors of antibiotics: A review. J. Hazard.
860 Mater. 459, 132279. https://doi.org/10.1016/j.jhazmat.2023.132279
861 Liaoning Provincial Marine Ecological Early Warning Monitoring Bulletin (2023),

2024. https://zrzy.ln.gov.cn/zrzy/ywbb/gzkx/20240829143003950 09/index.shtml

Lin, B., Pan, F., 2023. Applications of DGT in coastal sediments: monitoring and biogeochemical study of trace metals and oxyanions. Trends Environ. Anal. Chem. 39, e00207. https://doi.org/10.1016/j.teac.2023.e00207

Liu, W., Lu, G., Wang, W.-X., 2022a. *In situ* high-resolution two-dimensional profiles of redox sensitive metal mobility in sediment-water interface and porewater from estuarine sediments. Sci. Total Environ. 820, 153034. https://doi.org/10.1016/j.scitotenv.2022.153034

Liu, Y., Sun, Y., Yu, J., Xia, X., Ding, A., Zhang, D., 2022b. Impacts of groundwater level fluctuation on soil microbial community, alkane degradation efficiency and alkane-degrading gene diversity in the critical zone: Evidence from an accelerated water table fluctuation simulation. Environ. Sci. Pollut. Res. 29, 83060–83070. https://doi.org/10.1007/s11356-022-21246-2

Lu, J., Liu, T., Zhang, X., Gao, R., Liu, Y., 2021. A dynamic flux model for analyses of phosphorus exchange between overlying water and sedimentary deposits of a reservoir in the cold area of north China. Ecol. Eng. 161, 106116. https://doi.org/10.1016/j.ecoleng.2020.106116

Luo, D., Guo, Y., Liu, Z., Guo, L., Wang, H., Tang, X., Xu, Z., Wu, Y., Sun, X., 2024. Endocrine-Disrupting Chemical Exposure Induces Adverse Effects on the Population Dynamics of the Indo-Pacific Humpback Dolphin. Environ. Sci. Technol. 58, 9102–9112. https://doi.org/10.1021/acs.est.4c00618

883 Ma, J., Zhou, Z., Guo, Q., Zhu, S., Dai, Y., Shen, Q., 2019. Spatial Characterization of
884 Seawater Intrusion in a Coastal Aquifer of Northeast Liaodong Bay, China.
885 Sustainability 11, 7013. https://doi.org/10.3390/su11247013
886 Ma, Y., Hu, A., Yu, C.-P., Yan, Q., Yan, X., Wang, Y., Deng, F., Xiong, H., 2015.
887 Response of microbial communities to bioturbation by artificially introducing
888 macrobenthos to mudflat sediments for in situ bioremediation in a typical semi-
889 enclosed bay, southeast China. Mar. Pollut. Bull. 94, 114–122.
890 https://doi.org/10.1016/j.marpolbul.2015.03.003
891 Ma, Y., Hua, Z., Wang, P., Yang, Y., Dong, Y., Yu, L., 2023. Mechanisms of propeller
892 jet-induced migration, release, and distribution of perfluoroalkyl acids in
893 sediment–water systems. Water Res. 238, 120048.
894 https://doi.org/10.1016/j.watres.2023.120048
895 Meng, Q., Zhang, W., Zhou, F., Liao, Y., Yu, P., Tang, Y., Ma, X., Tian, D., Ding, R., Ni,
896 X., Zeng, D., Schrum, C., 2022. Water Oxygen Consumption Rather Than
897 Sediment Oxygen Consumption Drives the Variation of Hypoxia on the East China
898 Sea Shelf. J. Geophys. Res. Biogeosciences 127, e2021JG006705.
899 https://doi.org/10.1029/2021JG006705
900 Mengel, M., Levermann, A., Frieler, K., Robinson, A., Marzeion, B., Winkelmann, R.,
901 2016. Future sea level rise constrained by observations and long-term commitment.
902 Proc. Natl. Acad. Sci. 113, 2597–2602. https://doi.org/10.1073/pnas.1500515113
903 Mondal, P., Walter, M., Miller, J., Epanchin-Niell, R., Gedan, K., Yawatkar, V., Nguyen,

E., Tully, K.L., 2023. The spread and cost of saltwater intrusion in the US Mid-Atlantic. Nat. Sustain. 6, 1352–1362. https://doi.org/10.1038/s41893-023-01186-6

Omar, T.F.T., Aris, A.Z., Yusoff, F.Md., Mustafa, S., 2017. An improved SPE-LC-MS/MS method for multiclass endocrine disrupting compound determination in tropical estuarine sediments. Talanta 173, 51–59. https://doi.org/10.1016/j.talanta.2017.05.064

Pan, F., Cai, Y., Guo, Z., Fu, Y., Wu, X., Liu, H., Wang, X., 2021. Kinetic characteristics of mobile Mo associated with Mn, Fe and S redox geochemistry in estuarine sediments. J. Hazard. Mater. 418, 126200. https://doi.org/10.1016/j.jhazmat.2021.126200

Paolella, G., Fabbricino, M., Locascio, A., Sirakov, M., Pontoni, L., 2024. Fate of bisphenol A in marine environment: a critical review. Chem. Eng. J. 495, 153228. https://doi.org/10.1016/j.cej.2024.153228

Pastorino, P., Barceló, D., Prearo, M., 2024. Alps at risk: High-mountain lakes as reservoirs of persistent and emerging contaminants. J. Contam. Hydrol. 264, 104361. https://doi.org/10.1016/j.jconhyd.2024.104361

Puttonen, I., Lukkari, K., Miettunen, E., Ropponen, J., Tuomi, L., 2024. Estimating internal phosphorus loading for a water quality model using chemical characterisation of sediment phosphorus and contrasting oxygen conditions. Sci. Total Environ. 942, 173717. https://doi.org/10.1016/j.scitotenv.2024.173717

925 Qiu, W., Chen, J., Li, Y., Chen, Z., Jiang, L., Yang, M., Wu, M., 2016. Oxidative stress
926 and immune disturbance after long-term exposure to bisphenol A in juvenile
927 common carp (Cyprinus carpio). Ecotoxicol. Environ. Saf. 130, 93–102.
928 https://doi.org/10.1016/j.ecoenv.2016.04.014
929 Quintero, I., Castillo, A., Mejía, L., 2022. Diversity and Taxonomy of Soil Bacterial
930 Communities in Urban and Rural Mangrove Forests of the Panama Bay.
931 Microorganisms 10, 2191. https://doi.org/10.3390/microorganisms10112191
932 Reif, D., Zoboli, O., Wolfram, G., Amann, A., Saracevic, E., Riedler, P., Hainz, R.,
933 Hintermaier, S., Krampe, J., Zessner, M., 2022. Pollutant source or sink?
934 Adsorption and mobilization of PFOS and PFOA from sediments in a large
935 shallow lake with extended reed belt. J. Environ. Manage. 320, 115871.
936 https://doi.org/10.1016/j.jenvman.2022.115871
937 Romanenko, L., Otstavnykh, N., Kurilenko, V., Velansky, P., Baldaev, S., Mikhailov, V.,
938 Isaeva, M., 2022. Marinobacterium sedimentorum sp. nov., Isolated from the
939 Bottom Sediments of the Okhotsk Sea. Diversity 14, 944.
940 https://doi.org/10.3390/d14110944
941 Safakhah, N., Ghanemi, K., Nikpour, Y., Batvandi, Z., 2020. Occurrence, distribution,
942 and risk assessment of bisphenol A in the surface sediments of Musa estuary and
943 its tributaries in the northern end of the Persian Gulf, Iran. Mar. Pollut. Bull. 156,
944 111241. https://doi.org/10.1016/j.marpolbul.2020.111241
945 Saintilan, N., Kovalenko, K.E., Guntenspergen, G., Rogers, K., Lynch, J.C., Cahoon,

946 D.R., Lovelock, C.E., Friess, D.A., Ashe, E., Krauss, K.W., Cormier, N., Spencer,
947 T., Adams, J., Raw, J., Ibanez, C., Scarton, F., Temmerman, S., Meire, P., Maris,
948 T., Thorne, K., Brazner, J., Chmura, G.L., Bowron, T., Gamage, V.P., Cressman,
949 K., Endris, C., Marconi, C., Marcum, P., St Laurent, K., Reay, W., Raposa, K.B.,
950 Garwood, J.A., Khan, N., 2022. Constraints on the adjustment of tidal marshes to
951 accelerating sea level rise. Science 377, 523–527.
952 https://doi.org/10.1126/science.abo7872
953 Savvichev, A.S., Rusanov, I.I., Kadnikov, V.V., Beletsky, A.V., Zakcharova, E.E.,
954 Samylina, O.S., Sigalevich, P.A., Semiletov, I.P., Ravin, N.V., Pimenov, N.V., 2023.
955 Biogeochemical Activity of Methane-Related Microbial Communities in Bottom
956 Sediments of Cold Seeps of the Laptev Sea. Microorganisms 11, 250.
957 https://doi.org/10.3390/microorganisms11020250
958 Schuerch, M., Spencer, T., Temmerman, S., Kirwan, M.L., Wolff, C., Lincke, D.,
959 McOwen, C.J., Pickering, M.D., Reef, R., Vafeidis, A.T., Hinkel, J., Nicholls, R.J.,
960 Brown, S., 2018. Future response of global coastal wetlands to sea-level rise.
961 Nature 561, 231–234. https://doi.org/10.1038/s41586-018-0476-5
962 Stigebrandt, A., Rahm, L., Viktorsson, L., Ödalen, M., Hall, P.O.J., Liljebladh, B., 2014.
963 A New Phosphorus Paradigm for the Baltic Proper. AMBIO 43, 634–643.
964 https://doi.org/10.1007/s13280-013-0441-3
965 Su, X., Befus, K.M., Hummel, M.A., 2024. Shoreline barriers may amplify coastal
966 groundwater hazards with sea-level rise. Sci. Rep. 14, 15559.

https://doi.org/10.1038/s41598-024-66273-w

Suárez-Moo, P., Lamelas, A., Garcia-Bautista, I., Barahona-Pérez, L.F., Sandoval-Flores, G., Valdes-Lozano, D., Toledano-Thompson, T., Polanco-Lugo, E., Valdez-Ojeda, R., 2020. Characterization of sediment microbial communities at two sites with low hydrocarbon pollution in the southeast Gulf of Mexico. PeerJ 8, e10339. https://doi.org/10.7717/peerj.10339

Sun, K., Gao, B., Zhang, Z., Zhang, G., Liu, X., Zhao, Y., Xing, B., 2010. Sorption of endocrine disrupting chemicals by condensed organic matter in soils and sediments. Chemosphere 80, 709–715. https://doi.org/10.1016/j.chemosphere.2010.05.028

Sun, W., Yu, G., Louie, T., Liu, T., Zhu, C., Xue, G., Gao, P., 2015. From mesophilic to thermophilic digestion: the transitions of anaerobic bacterial, archaeal, and fungal community structures in sludge and manure samples. Appl. Microbiol. Biotechnol. 99, 10271–10282. https://doi.org/10.1007/s00253-015-6866-9

Tang, G., Yang, M., Chen, Xiaohong, Jiang, T., Chen, T., Chen, Xiaohua, Fang, H., 2020. A new idea for predicting and managing seawater intrusion in coastal channels of the Pearl River, China. J. Hydrol. 590, 125454. https://doi.org/10.1016/j.jhydrol.2020.125454

Tiwari, M., Sahu, S.K., Pandit, G.G., 2016. Distribution and estrogenic potential of endocrine disrupting chemicals (EDCs) in estuarine sediments from Mumbai, India. Environ. Sci. Pollut. Res. 23, 18789–18799.

https://doi.org/10.1007/s11356-016-7070-x

Van Ael, E., Covaci, A., Das, K., Lepoint, G., Blust, R., Bervoets, L., 2013. Factors Influencing the Bioaccumulation of Persistent Organic Pollutants in Food Webs of the Scheldt Estuary. Environ. Sci. Technol. 47, 11221–11231. https://doi.org/10.1021/es400307s

van de Pol, M., Bailey, L.D., Frauendorf, M., Allen, A.M., van der Sluijs, M., Hijner, N., Brouwer, L., de Kroon, H., Jongejans, E., Ens, B.J., 2024. Sea-level rise causes shorebird population collapse before habitats drown. Nat. Clim. Change 14, 839–844. https://doi.org/10.1038/s41558-024-02051-w

van Erk, M.R., Bourceau, O.M., Moncada, C., Basu, S., Hansel, C.M., de Beer, D., 2023. Reactive oxygen species affect the potential for mineralization processes in permeable intertidal flats. Nat. Commun. 14, 938. https://doi.org/10.1038/s41467-023-35818-4

Walker, A.M., Leigh, M.B., Mincks, S.L., 2023. Benthic bacteria and archaea in the North American Arctic reflect food supply regimes and impacts of coastal and riverine inputs. Deep Sea Res. Part II Top. Stud. Oceanogr. 207, 105224. https://doi.org/10.1016/j.dsr2.2022.105224

Wang, B., Dong, F., Chen, S., Chen, M., Bai, Y., Tan, J., Li, F., Wang, Q., 2016. Phenolic endocrine disrupting chemicals in an urban receiving river (Panlong river) of Yunnan–Guizhou plateau: Occurrence, bioaccumulation and sources. Ecotoxicol. Environ. Saf. 128, 133–142. https://doi.org/10.1016/j.ecoenv.2016.02.018

1009 Wang, C., Mao, Y., Zhang, L., Wei, H., Wang, Z., 2024a. Insight into environmental
1010 adaptability of antibiotic resistome from surface water to deep sediments in
1011 anthropogenic lakes by metagenomics. Water Res. 256, 121583.
1012 https://doi.org/10.1016/j.watres.2024.121583
1013 Wang, Q., Tsui, M.M.P., Ruan, Y., Lin, H., Zhao, Z., Ku, J.P.H., Sun, H., Lam, P.K.S.,
1014 2019a. Occurrence and distribution of per- and polyfluoroalkyl substances (PFASs)
1015 in the seawater and sediment of the South China sea coastal region. Chemosphere
1016 231, 468–477. https://doi.org/10.1016/j.chemosphere.2019.05.162
1017 Wang, X., Liu, J., Li, B., Liang, J., Sun, H., Zhou, S., Zhang, X.-H., 2019b. Spatial
1018 Heterogeneity of Vibrio spp. in Sediments of Chinese Marginal Seas. Appl.
1019 Environ. Microbiol. 85, e03064-18. https://doi.org/10.1128/AEM.03064-18
1020 Wang, X.-C., Yue, F.-J., Li, S.-L., Li, X.-Z., Lang, Y.-C., Hu, J., Ding, H., Liu, C.-Q.,
1021 2022. Spatial variations in water chemical components in a coastal zone of
1022 northern China: Insights from environmental isotopes. J. Hydrol. 612, 128054.
1023 https://doi.org/10.1016/j.jhydrol.2022.128054
1024 Wang, Y., Hu, Y., Liu, Y., Chen, Q., Xu, J., Zhang, F., Mao, J., Shi, Q., He, C., Cai, R.,
1025 Lønborg, C., Liu, L., Guo, A., Jiao, N., Zheng, Q., 2024b. Heavy metal induced
1026 shifts in microbial community composition and interactions with dissolved
1027 organic matter in coastal sediments. Sci. Total Environ. 927, 172003.
1028 https://doi.org/10.1016/j.scitotenv.2024.172003
1029 Wu, G., Shang, J., Pan, L., Wang, Z., 2014. Heavy metals in surface sediments from

1030 nine estuaries along the coast of Bohai Bay, Northern China. Mar. Pollut. Bull. 82,
1031 194–200. https://doi.org/10.1016/j.marpolbul.2014.02.033
1032 Wu, M., Xu, H., Shen, Y., Qiu, W., Yang, M., 2011. Oxidative stress in zebrafish
1033 embryos induced by short-term exposure to bisphenol A, nonylphenol, and their
1034 mixture. Environ. Toxicol. Chem. 30, 2335–2341. https://doi.org/10.1002/etc.634
1035 Wu, Y., Zhou, Z., Fu, H., Zhang, P., Zheng, Y., 2022. Metagenomic analysis of microbial
1036 community and gene function of anodic biofilm for nonylphenol removal in
1037 microbial fuel cells. J. Clean. Prod. 374, 133895.
1038 https://doi.org/10.1016/j.jclepro.2022.133895
1039 Xiao, Y., Han, D., Currell, M., Song, X., Zhang, Y., 2023. Review of Endocrine
1040 Disrupting Compounds (EDCs) in China's water environments: Implications for
1041 environmental fate, transport and health risks. Water Res. 245, 120645.
1042 https://doi.org/10.1016/j.watres.2023.120645
1043 Xiong, G., Zhu, X., Wu, J., Liu, M., Yang, Y., Zeng, X., 2023. Seawater intrusion alters
1044 nitrogen cycling patterns through hydrodynamic behavior and biochemical
1045 reactions: Based on Bayesian isotope mixing model and microbial functional
1046 network. Sci. Total Environ. 867, 161368.
1047 https://doi.org/10.1016/j.scitotenv.2022.161368
1048 Xu, E.G., Chan, S.N., Choi, K.W., Lee, J.H.W., Leung, K.M.Y., 2018. Tracking major
1049 endocrine disruptors in coastal waters using an integrative approach coupling
1050 field-based study and hydrodynamic modeling. Environ. Pollut. 233, 387–394.

https://doi.org/10.1016/j.envpol.2017.10.086

Yan, D., Huang, Y., Wang, Z., Chen, Q., Zhang, J., Dong, J., Fan, Z., Yan, H., Mao, F., 2022. Key role of suspended particulate matter in assessing fate and risk of endocrine disrupting compounds in a complex river-lake system. J. Hazard. Mater. 431, 128543. https://doi.org/10.1016/j.jhazmat.2022.128543

Yu, H., Zhong, Q., Peng, Y., Zheng, X., Xiao, F., Wu, B., Yu, X., Luo, Z., Shu, L., Wang, C., Yan, Q., He, Z., 2022. Environmental Filtering by pH and Salinity Jointly Drives Prokaryotic Community Assembly in Coastal Wetland Sediments. Front. Mar. Sci. 8, 792294. https://doi.org/10.3389/fmars.2021.792294

Yu, K., Yi, S., Li, B., Guo, F., Peng, X., Wang, Z., Wu, Y., Alvarez-Cohen, L., Zhang, T., 2019. An integrated meta-omics approach reveals substrates involved in synergistic interactions in a bisphenol A (BPA)-degrading microbial community. Microbiome 7, 16. https://doi.org/10.1186/s40168-019-0634-5

Yuan, K., Xiao, S., Jiang, X., Yang, L., Chen, B., Luan, T., Lin, L., Tam, N.F.Y., 2017b. Effects of endocrine disrupting chemicals (EDCs) on bacterial communities in mangrove sediments. Mar. Pollut. Bull. 122, 122–128. https://doi.org/10.1016/j.marpolbul.2017.06.035

Yuan, X., Yang, X., Zhang, A., Ma, X., Gao, H., Na, G., Zong, H., Liu, G., Sun, Y., 2017a. Distribution, potential sources and ecological risks of two persistent organic pollutants in the intertidal sediment at the Shuangtaizi Estuary, Bohai Sea of China. Mar. Pollut. Bull. 114, 419–427.

https://doi.org/10.1016/j.marpolbul.2016.09.058

Zainuddin, A.H., Roslan, M.Q.J., Razak, M.R., Yusoff, F.Md., Haron, D.E.M., Aris, A.Z., 2023. Occurrence, distribution, and ecological risk of bisphenol analogues in marine ecosystem of urbanized coast and estuary. Mar. Pollut. Bull. 192, 115019. https://doi.org/10.1016/j.marpolbul.2023.115019

Zeng, B., Wu, Y., Huang, Y., Colucci, M., Bancaro, N., Maddalena, M., Valdata, A., Xiong, X., Su, X., Zhou, X., Zhang, Z., Jin, Y., Huang, W., Bai, J., Zeng, Y., Zou, X., Zhan, Y., Deng, L., Wei, Q., Yang, L., Alimonti, A., Qi, F., Qiu, S., 2024. Carcinogenic health outcomes associated with endocrine disrupting chemicals exposure in humans: A wide-scope analysis. J. Hazard. Mater. 476, 135067. https://doi.org/10.1016/j.jhazmat.2024.135067

Zhang, H., Zheng, S., Ding, J., Wang, O., Liu, F., 2017. Spatial variation in bacterial community in natural wetland-river-sea ecosystems. J. Basic Microbiol. 57, 536–546. https://doi.org/10.1002/jobm.201700041

Zhang, L., Wu, Y., Ni, Z., Li, J., Ren, Y., Lin, J., Huang, X., 2023a. Saltwater intrusion regulates the distribution and partitioning of heavy metals in water in a dynamic estuary, South China. Mar. Environ. Res. 186, 105943. https://doi.org/10.1016/j.marenvres.2023.105943

Zhang, X., Gao, Y., Li, Q., Li, G., Guo, Q., Yan, C., 2011. Estrogenic Compounds and Estrogenicity in Surface Water, Sediments, and Organisms from Yundang Lagoon in Xiamen, China. Arch. Environ. Contam. Toxicol. 61, 93–100.

https://doi.org/10.1007/s00244-010-9588-0

Zhang, X., Geng, K., Wu, N., Hu, G., Fan, B., He, J., Qiao, W., 2023b. Sustained anaerobic degradation of 4-chloro-2-methylphenoxyacetic acid by acclimated sludge in a continuous-flow reactor. Chemosphere 330, 138749. https://doi.org/10.1016/j.chemosphere.2023.138749

Zhang, X., Li, Q., Li, G., Wang, Z., Yan, C., 2009. Levels of estrogenic compounds in Xiamen Bay sediment, China. Mar. Pollut. Bull. 58, 1210–1216. https://doi.org/10.1016/j.marpolbul.2009.03.011

Zhang, Y., Yao, P., Sun, C., Li, S., Shi, X., Zhang, X.-H., Liu, J., 2021. Vertical diversity and association pattern of total, abundant and rare microbial communities in deep-sea sediments. Mol. Ecol. 30, 2800–2816. https://doi.org/10.1111/mec.15937

Zhao, Z., Zhang, L., Zhang, G., Gao, H., Chen, X., Li, L., Ju, F., 2023. Hydrodynamic and anthropogenic disturbances co-shape microbiota rhythmicity and community assembly within intertidal groundwater-surface water continuum. Water Res. 242, 120236. https://doi.org/10.1016/j.watres.2023.120236

Zoppini, A., Ademollo, N., Patrolecco, L., Langone, L., Lungarini, S., Dellisanti, W., Amalfitano, S., 2018. Distribution patterns of organic pollutants and microbial processes in marine sediments across a gradient of anthropogenic impact. Environ. Pollut. 242, 1860–1870. https://doi.org/10.1016/j.envpol.2018.07.081

Zoppini, A., Bongiorni, L., Ademollo, N., Patrolecco, L., Cibic, T., Franzo, A., Melita, M., Bazzaro, M., Amalfitano, S., 2020. Bacterial diversity and microbial

functional responses to organic matter composition and persistent organic pollutants in deltaic lagoon sediments. Estuar. Coast. Shelf Sci. 233, 106508. https://doi.org/10.1016/j.ecss.2019.106508